Incorporation of In Vitro Double Seeding for Enhanced Development of Tissue Engineered Skeletal Muscle Implants

_____

A Thesis

Presented to

The faculty of School of Engineering and Applied Science

University of Virginia

_____

in partial fulfillment

of requirements for the degree

Master of Science

by

Kimberly Smith

December

2019

The thesis

is submitted in partial fulfillment of the requirements

for the degree of

Master of Science

Kimberly Smith

AUTHOR

The thesis as been read and approved by the examining committee:

George Christ .
Advisor

Shayn Peirce-Cottler

Donald Griffin .

Accepted for the School of Engineering and Applied Science:

Craig H. Benson, Dean, School of Engineering and Applied Science
December
2019

Introduction and Rationale

a. Need for regenerative medicine and tissue engineering

Regenerative medicine may be defined as the process of re-growing, repairing, or replacing traumatically or genetically damaged tissue to restore normal function. Therapeutic methods typically employ stem cells or tissue engineering techniques, sometimes a combination of both, to incite the body's endogenous repair mechanisms to heal tissues and organs, or to replace the damaged organ entirely. Regenerative medicine poses the potential to grow tissues and organs in the laboratory and safely implant them until the body is able to heal itself[1,2]. The aging baby boomer population and rapid development of transplant medicine results in an increased demand for tissues and organs far exceeding available donor organs. Furthermore, while medical advancements in transplant technology allow for survival of previously fatal conditions and injuries, current transplant techniques contribute to an escalation of donor and recipient site tissue morbidity accompanied by functional and aesthetic defects. Current estimates suggest that regenerative medicine could significantly counterbalance this deficit of donor organs and reduce the occurrence of donor and recipient site tissue morbidity[2]. For less severe injuries, such as battlefield injuries and civilian accidents, total organ replacement may not be required. Regenerative medicine constructs can be implanted into wound beds to incite or accelerate natural healing responses that otherwise would not be sufficient to restore function or appearance of the wound. The massive potential impact of widespread regenerative medicine technology implementation has been recognized by Manufacturing USA and the Department of Defense with the recent founding of the Advanced Regenerative Manufacturing Institute (ARMI), a centralized consortium focused on turning laboratory breakthroughs into manufactured products.[4]

b. Skeletal muscle engineering and TEMR

Our lab has developed a tissue-engineered muscle repair (TEMR) construct technology which specifically addresses soft tissue, skeletal muscle tissue engineering. The TEMR technology has shown great promise in preclinical studies, and our group has submitted an IND application to support implementation in a "first in man" pilot study. However, further characterization and refinement of the TEMR and the injury response after implantation are required for a more widespread clinical application. A previous observation in our lab noted that increased cell seeding could yield improved functional recovery in animal models and was the inspiration to study the second generation TEMR, or TEMR II[3]. Additionally, we wanted to study this technology in an immune-competent model that more closely mimics human implant response. To this end, this thesis has focused on the following:

c. What thesis will focus on

i. Improving bioreactor design for re-seeding process
ii. Advancing TEMR to the second generation TEMR II technology, delivering more cells to the wound bed

iii. Functional recovery following implantation in a biologically relevant skeletal muscle traumatic injury model for extended time points – up to 6 months

We consider the rationale of each of these briefly below, and discuss them in much more detail in the body of the thesis.

d. Hurdles that we address

a. <u>The re-seeding problem: improving bioreactor</u>

The first hurdle to overcome lies in the optimization of the in vitro development of the TEMR technology. Efforts within this segment are largely focused on improving the consistent maneuverability of scaffolds. Specifically, we will examine the development of a new bioreactor system that allows all TEMR construct within the bioreactor to be simultaneously removed, flipped 180° and placed back in the bioreactor with minimal disturbance to the cell layers present on either surface of the TEMR scaffold.

b. <u>Re-seeding</u>

The co-delivery of acellular scaffolds and muscle progenitor cells (MPCs) reduces the injured tissue burden of regenerating extracellular matrix as the scaffold effectively provides a myoconductive microenvironment in wound, and the MPCs serve as a myogenic cell source to the defect space[4]. More importantly, however, are the promising functional recoveries repeatedly demonstrated by these technologies[5,6], sometimes yielding 60-70% functional recovery when compared to uninjured control tissue. As encouraging as these initial findings are, there is still significant room for improvement in total functional recovery. In a previous study done in our lab[3], double seeded TEMRs (TEMR IIs), demonstrated accelerated and prolonged recovery. While this was certainly a step in the right direction, the herein presented study seeks to advance the TEMR II technology by evaluating its regenerative potential in 1) a larger and more clinically-relevant injury model in the rat latissimus (LD) dorsi; 2) an animal model with uncompromised immune system, given the importance of immune system during the regenerative process[7], 3) over an extended period of time (2, 4 and 6 month after injury), to fully understand the long-term functional effects of a densely seeded, preconditioned TEMR construct on VML injury.

c. <u>Functional and aesthetic improvement</u>

The overriding hypothesis of this study was that TEMR IIs, made possible by specialized bioreactor preconditioning, would yield significant long-term functional improvements to large VML injuries in immune competent animal models. To this end, VML injuries, with or without the implanted TEMR II technology, were examined in an established rat LD VML model for their ability to enable restoration of function and native tissue morphology.

Incorporation of In Vitro Double Seeding for Enhanced Development of Tissue Engineered Skeletal Muscle Implants

1. Chapter 1 – Skeletal muscle, Tissue Engineering, and Current Treatments for VML

Introduction

Skeletal muscle is estimated to make up 30-40% of an average adult's body composition, making it one of the most abundant tissues in the human body[8]. It is necessary for generating force for voluntary movement, and critical loss of this tissue results in functional and cosmetic deficits that reduce quality of life. Skeletal muscle has an extraordinary capacity to repair itself after injury with the help of satellite cells[9], but in cases of major trauma and extreme muscle loss, these repair mechanisms fail. Soft tissue trauma that results in an irrecoverable muscle loss beyond the body's endogenous repair capacity is defined as volumetric muscle loss, or VML[10]. Most of combat injuries result in this frank loss of skeletal muscle in the head, neck, and extremities[11]. Frequent reasons VML injuries in civilian populations are car accidents, sports injuries, gunshot wounds, surgical debridement, congenital birth defects, and acquired disease[12–14]. The widespread incidence of VML in both civilian and military populations, coupled with the severity of its indications and lack of effective treatment, urgently demand improved therapeutic treatments.

1.1 Skeletal muscle physiology and anatomy

The skeletal muscle is composed of several hierarchical units, neatly ordered and registered such that they give the tissue a striated appearance under a microscope. The primary sub-cellular unit of the skeletal muscle are microscopic sarcomeres comprised of actin and myosin filaments. Comparatively large myosin filaments exhibit myosin heads that can bind to actin when troponin is removed. When sarcomeres are arranged in series, they form myofibrils. Myofibrils packed together in parallel form a myofiber, which is neatly wrapped in sarcolemma. This is the basic functional unit of skeletal muscle as it consists of the physiological and structural mechanisms required for muscle stimulation and contraction. Myofibers and their sarcolemma coverings are bound and delineated from one another by endomysium, a connective tissue composed of collagen and proteoglycans. Many myofibers bound together by the endomysium-comparable connective tissue called perimysium is known as a fascicle. Finally, groups of fascicles form the actual muscle body and are wrapped by an epimysium. All of these layers are covered by an extracellular matrix (ECM) known as fascia, and all together form a deformable structure that can support passive load[15,16].

1.1.1 Excitation contraction coupling

Activation and contraction of skeletal muscle happens at the myofiber level, where each individual sarcomere contracts a microscopic distance. A chemical synapse formed by contact between a motor neuron and a myofiber, called a neuromuscular junction, is the site in which a motor neuron transmits a chemical signal to a muscle fiber. Release of this chemical signal, acetocholine, triggers an action potential that travels down t-tubules and into the myofibers. This depolarizes the muscle fiber and opens voltage-gated ion channels in the sarcolemma. These ion channels are physically

linked to calcium channels in the sarcoplasmic reticulum of the cell, and when they are opened calcium rushes into the bulk cytosol of the cell. Calcium binds to troponin C on actin filaments, moving it out of the way as to expose active sites on the actin. Myosin heads can then bind to the active sits on actin filaments. When a myosin head binds to actin, the adenosine diphosphate (ADP) responsible for cocking the myosin head is ejected and the myosin head pivots, pulling the actin filaments toward the center of the sarcomere parallel to the myosin filaments. This produces force and, in some cases, contraction. The hydrolysis of an adenosine triphosphate (ATP) onto the myosin heads re-cocks the heads, resetting the myosin for further contraction. As long as active sites remain exposed on actin filaments and ATP is available for re-setting myosin heads, sarcomeres will continue to contract[15,16].

1.1.2 Skeletal muscle wound healing

When searching for alternative therapeutic options for VML injuries, we must first consider mimicking the degeneration-regeneration cycle intrinsic to healthy muscle. Briefly, after physical damage to the muscle cell, endogenous enzyme proteases released from macrophages immediately begin to digest damaged cellular components[15,16]. Next, satellite cells present along the periphery of muscle fibers begin to proliferate. At high enough densities, satellite cells soon begin to express regulatory factors such as MyoD that indicate their commitment to myogenic lineage[17], then they align along basal lamina and fuse into myotubes. The role of basal lamina (largely collagen), is well known to be of critical importance to satellite cell proliferation and fusion, and it may promote the myogenic lineage of satellite cells by expressing various extracellular matrix components[15,18]. As regeneration continues and myotubes mature, they begin to synthesize contractile proteins. Myonuclei are usually pushed to the periphery of the cell, but in some instances the nucleus remains in the center and serves as a pathological marker for cells that have undergone regeneration[15].

This strategy works extremely well for relatively small gaps in the muscle continuity following injury and trauma as in the case in exercise or small lacerations. However, in surgeries, traumatic injuries and congenital defects where significant amounts of muscle, vessel, nerves, and ECM are simultaneously damaged or missing, the body is incapable of restoring the tissue because the damage sustained exceeds the body's endogenous capacity for regeneration. This incomplete recovery of the structure and functionality of muscle is the phenotype for VML injuries and can generally be described by loss of at least 10% muscle mass in a given location[6].

With respect to the endogenous degeneration-regeneration cycle, tissue engineering (TE) research studies aimed at VML repair have utilized acellular biological scaffolds with co-delivery of cells[19–26]. The co-delivery of acellular scaffolds and muscle progenitor cells (MPCs) reduces the injured tissue burden of re-generating extracellular matrix as the scaffold effectively provides a myoconductive microenvironment in wound, and the MPCs serve as a myogenic cell source to the defect space[4]. More importantly, however, are the promising functional recoveries repeatedly demonstrated by these technologies[5,6], sometimes yielding 60-70% functional recovery when compared to uninjured control tissue. The purpose of this thesis is to review and expound upon these implantable therapeutic treatments for the functional and cosmetic recovery of skeletal muscle.

When evaluating TE implantable devices as therapeutic treatments, what are the metrics of success? We can use the easily recognizable functional and structural hallmarks of healthy skeletal muscle as a gold standard. Specifically, the ideal outcome for regenerated tissue post TE treatment should exhibit functional contractile elements, fiber alignment, vasculature, and neural coupling. While various groups have had some success generating muscle constructs in vitro that possess several of these characteristics, none have successfully recapitulated all of these elements.

1.2 Applications of in vitro tissue engineered skeletal muscle

What are the benefits and advantages to creating *in vitro* TE skeletal muscle? The first is to facilitate the study of muscle tissue damage and repair *in vitro*. The mechanisms that govern the endogenous degeneration-regeneration response in damaged skeletal muscle can, in part, be dissected and studied using *in vitro* TE skeletal constructs[29]. Second, these models can be used for drug and toxicity testing, and can also be used to assess the efficacy of certain personalized medicine therapies[27]. Third, TE of skeletal muscle can be used as a tissue fabrication technology for the generation of large bio-artificial muscle for soft robotics[28,29]. Finally, and perhaps most poignantly for this thesis, TE skeletal muscle can be used for the creation of implantable regenerative constructs that facilitate muscle regeneration *in vivo*[3,5,6,30,31].

There exist several philosophies of TE skeletal muscle implant design for use in muscle regeneration *in vivo*. The ideal TE muscle implant would be a mature, native-like phenotype of contractile muscle that includes functional vasculature, neural innervation, chemical signaling and mechanical connection. This level of TE skeletal construct has yet to be achieved. However, there exist "stepping stone" technologies that aim to mimic some of the biologically relevant features of mature muscle phenotype constructs.

The simplest technology is a transfer construct, where TE muscle tissue scaffold can be implanted subcutaneously. The construct uses native environment to grow and mature, and is then removed and employed as an autologous muscle graft[32]. This kind of technology is limited because as the tissue engineered implant grows it integrates with the native tissue. Removing the matured implant damages the native tissue, thus this process is not scalable as it is directly limited by the healthy tissue available for implant maturation. Furthermore, limited vascular integration into an implant creates ischemic conditions that favor fibroblast formation and growth[33]. To circumvent these issues, we focus on a new idea: an implant that encourages the body to regenerate on its own.

The second technology, and the focus of this thesis, uses the implantation of a phenotypically immature construct developed *in vitro* that stimulates the generation of new tissue by engaging the body's endogenous repair mechanisms. Investigators have evaluated many combinations and permutations of *in vitro* conditions, but in this thesis, we specifically look to assess the impact of MPC cell density in seeded constructs on functional recovery *in vivo*.

Successful TE therapeutic strategies require integration with native tissue and cells through appropriate cellular signals. Therefore, inclusion of biologically active DNA is critical to success[34]. Combined delivery of cells together with biologically relevant cell delivery vehicles has the potential to enhance, modulate, or even initiate local or systemic repair processes, increasing efficiency for regenerative medicine applications[35]. Ideally, biomaterials used as cell delivery

vehicles in *in vitro* TE tissue technologies provide cells with topological, chemical, and mechanical cues in the absence of native ECM until the cells can produce their own ECM[36,37]. The criteria for selecting biomaterials are based on chemistry, solubility, structure, hydrophobicity, and absorption/degradation. Ideal cell delivery vehicles must also present with biocompatibility, bioactivity, appropriate stiffness, and physiologically compatible biodegradation rates. Here, we highlight our decision to use a biological scaffold as an agent of cell delivery.

1.2.1 *Biological scaffolds*

The co-delivery of acellular scaffolds and progenitor cells reduces the injured tissue burden of re-generating extracellular matrix as the scaffold effectively provides a myoconductive microenvironment in the wound and prevents anoikis of co-delivered cells. Synthetic[38,39] and natural[40,41] scaffolds can be can be degradable or non-degradable, depending on the intended use.[42] Natural polymers were the first biodegradable biomaterials used clinically,[43] and their bioactive properties enhance cell interactions and make them ideal cell delivery vehicles. These scaffolds are particularly useful in that they effectively serve as biomechanical, biochemical, and structural analogs to native ECM; they bridge large gaps in endogenous ECM and integrate into endogenous tissue with little or no rejection. Their bioactive nature facilitates the maturation, proliferation, or differentiation of seeded cells which can, over time, excrete their own ECM to replace the acellular scaffold as it degenerates *in vivo*. Surgically implanted scaffolds that are seeded with cells can also contribute to a muscle body's passive resistance to being stretched, or its passive tension in areas previously rendered as having no passive force production due to a complete loss of any tissue or connective tissue.[44,45] These key features make scaffolds an ideal candidate for delivering cells and addressing functional recovery in VML wounds that require massive, simultaneous reconstitution of tissue and ECM.

1.3 Bioreactors in Skeletal Muscle Tissue Engineering

A bioreactor serves as a precise controller for mimicking the physiological environment that allow specified cells to grow[46]. Furthermore, bioreactor condition modulate the composition and mechanical properties of the engineered constructs[47]. There are various techniques used to obtain *de novo* tissue with biomechanical properties comparable to the desired tissue. Here, we briefly discuss *in vitro* bioreactors and highlight cyclic mechanical stretch bioreactors as ideal for our aims.

1.3.1 Perfusion

Flow perfusion bioreactors utilize a pump to continuously percolate media through a bioreactor and they may be a closed loop[48] or a closed, single-pass system[49]. The flow of media through the bioreactor significantly mitigates the diffusional limitations of traditional static culture[50]. Furthermore, fluid shear forces apply mechanical stimulation to cells and have been shown to increase mineral deposition and deliver better spatially-distributed extracellular matrix[51]. The use of perfusion bioreactors in skeletal muscle tissue engineering has been demonstrated to improve maturation and function of tissue engineered constructs[52,53].

1.3.2 Rotating Wall

This bioreactor was developed by NASA to create a microgravity culturing environment that could be simulated on earth or used in space[54]. It is made of two concentric cylinders, and the tissue construct floats freely between them. The inner cylinder rotates to create laminar media flow within the annular space, and the scaffold suspended within the annular space experiences the flow. This bioreactor has been used to create a more mature skeletal muscle construct, although not very recently[55,56].

1.3.3 Spinner Flask

Spinner flask bioreactors are used for growing suspension cultures in liquid media. Cell seeded scaffolds are suspended from the cover of a flask and submerged in culture medium. A magnetic stir bar placed at the bottom of the flask generates rotational force and "stirs" the media. This enhances oxygen diffusion and ensures greater tissue contact with nutrients compared to static culture[57,58]. This bioreactor technology has had limited success with skeletal muscle engineering, however[59]

1.3.4 Cyclic Mechanical Stretch

This thesis will focus on the use of cyclic mechanical stretch. It is well established that mechanical stimulation is critical to guiding muscle cell and connective tissue formation, organization, and growth, especially in comparison to unstretched counterparts.[60,61] Skeletal muscle and satellite cells in particular are sensitive to biophysical microenvironmental cues[62], especially mechanical loading[63,64]. Mechanical stretch increases proliferation and decreases differentiation, and simultaneously increases activity of cyclin-dependent kinase 2 (cdk2), cyclin A, and inhibits the expression of myosin heavy chain and formation of myotubes in C2C12 cultures[65]. Furthermore, in vitro mechanical conditioning has been used extensively in cell culture to replicate physiologically relevant muscle constructs. In myoblast cell culture, exposure to mechanical stretch stimuli has been shown to improve alignment, myofiber diameter, and skeletal muscle hypertrophy[66,67]. Mechanically loaded TE constructs often more closely mimic structural organization and force generation of native skeletal muscle[68]. Cyclic mechanical preconditioning improves engineered muscle contraction[68–70].

While the benefits of in vitro mechanical stimulation make the need for TE construct preconditioning obvious, there are multiple technologies to accomplish this goal. An investigation at the Harvard University tested a magnetically activated biphasic ferrogel scaffold implanted in the muscle to illicit uniform cyclic compression that ultimately led to reduced fibrous capsule formation around the implant and reduced fibrosis in the injured muscle[71]. More commonly, however, are the use of computer-controlled bioreactor systems[62,68,72,73]. Bioreactors have played a vital role in TE as they are capable of controlling several operational conditions including PH, temperature, perfusion, and mechanical forces[76]. Each bioreactor design can be highly tailored to mimic specific physiologically relevant conditions, and thus there are a wide spectrum of types of bioreactors. Herein, we begin with a bioreactor specifically designed for applying cyclic mechanical stretch to skeletal muscle constructs, and then we improve upon the design for maximizing efficiency and viability of in vitro re-seeding efforts.

1.3.5 TEMR Constructs

Recently, in vitro stretch preconditioning has been used in TE applications as is the case with the tissue-engineered muscle repair (TEMR) technology platform[3,5,68,72,74]. This technology begins with a decellularized, collagen-rich extracellular matrix derived from the lamina propria of a porcine bladder referred to as a bladder acellular matrix (BAM). The collagen-rich nature of the scaffold is robust and elastic enough to withstand bioreactor preconditioning (mechanical load and stretch) and surgical implantation[3,72,74,7531]. As described above, these BAMs serve as excellent compositional analogs to native skeletal ECM and are ideal cell delivery vehicles, particularly with respect to TE skeletal muscle constructs.

Following the decellularization process, BAMs are seeded in static culture with muscle progenitor cells (MPCs) isolated from mature muscle, affording the cells an opportunity to attach to the BAM. Seeded BAMs are subsequently subjected to cyclic mechanical preconditioning in a custom bioreactor, triggering the alignment and fusion of MPCs into multinucleated myotubes. These mechanically stretched, seeded scaffolds are known as TEMR constructs. Four distinct VML rodent studies have demonstrated significant in vivo regeneration post TEMR implantation. The first model surgically excised 50% of the latissimus dorsi (LD) to create a VML injury in female, immunosuppressed mice and sutured in the TEMR construct into the injury[74]. Force production measurements two months post-implantation yielded ~72% of maximal force capacity produced by native LD muscle ($p<0.05$). Furthermore, desmin-positive myofibers, blood vessels, and neurovascular bundles were all positively identified in the TEMR implant region[74]. A follow-up LD study developed a novel finite-element model for the evaluation of tissue engineering approaches of VML injuries in cranial muscles[31]. This study found that most of the force recovery is attributed to the passive mechanical properties of the tissue, despite significant muscle regeneration. The second model surgically resected 20% of the tibialis anterior (TA) muscle in male and female rats and generated ~61% of maximum functional capacity compared to native tissue three months post-implantation[72]. A TA follow-up study built directly on these observations and modified the geometry of the VML injury and the TEMR construct[76]. They observed ~62% functional recovery in a larger proportion of animals over 24 weeks. Furthermore, in ~25% of TEMR-implanted animals, recovery was virtually complete, highlighting the importance of tuning the application of tissue engineering technology to specific requirements of diverse VML injuries. These exciting results lead to further exploration of the potential regenerative capacity of the TEMR technology.

1.3.6 TEMR II Initial Data

It is reasonable to assume that if some preconditioned cells delivered on an acellular scaffold had significant functional recovery, a more densely seeded construct may yield increased functional and aesthetic improvements. One experiment[3] sought to determine the credibility to this line of logic. Similar to TEMR construct generation, a densely seeded TEMR (TEMR-2SPD) was created by seeding a BAM with MPCs in static culture and subsequently subjected to cyclic mechanical stretch in a computer-controlled bioreactor. The TEMRs were then re-seeded with MPCs again in static culture, and preconditioned in a bioreactor one last time, creating the TEMR-2SPD. It was

shown that VML injuries implanted with TEMR-2SPDs demonstrated accelerated and prolonged functional recovery, nearly double in magnitude when compared to TEMRs. While this was certainly a step in the right direction, there are certain deficiencies that this present study sought to address.

The most straightforward improvement of this study was using immune competent rats in favor of nude mice. An uncompromised immune system more closely resembles human injury – the eventual target of this technology. We are particularly interested in repair of the human adductor pollicis muscle of the hand as a springboard for our technology. The rat LD is comparable to that of the human adductor pollicis as they both exhibit a transverse and oblique head and a flat, triangular, fan-shaped body[77,78], and therefore is the perfect candidate for a rat LD model of injury. In addition, we extended the study to 2, 4, and 6-month time points in order to more fully understand the durability and long-term functional effects of a densely seeded, preconditioned construct on VML injury. The final, and perhaps most novel contribution of this study was the improved design of the bioreactor for seeding the acellular scaffolds. The new bioreactor design allowed each side of the BAM to be seeded twice with minimal disturbance to the initial layer of cells. Moreover, cells used for the second seeding were acquired from the same biopsy used to harvest the primary MPCs, allowing for the potential for increased functional recovery with minimal or no increase in muscle biopsy requirements.

1.4 Other methods for achieving cell alignment in vitro

Ideally, TE therapeutic implants would closely mimic or even match endogenous skeletal muscle architecture and function. As described above, the basic functional unit of mature skeletal muscle consists of fused myoblasts into myofibrils packed in parallel to form a myofiber. Thus, a key justification for the use of bioreactors in the preconditioning of skeletal muscle TE constructs is the alignment and fusion of MPCs into myotubes. The preconditioning process requires multiple days of cell culture and is not optimal for expedient treatment of acute injuries. There are, however, two additional methods for expedited cell alignment pre in vitro mechanical conditioning briefly explored in this study.

1.4.1 3D bio-printing and additive manufacturing

Additive manufacturing (AM) techniques in TE have the potential to overcome extensive, time-consuming in vitro culture required to fabricate constructs with accurate, three-dimensional design and stoichiometry. AM uses layer-by layer synthesis of printed material that circumvents traditional manufacturing hurdles such as internal porosities, residual stress, and interlocking shapes without connections[79]. When applied to TE, the bottom-up fabrication process allows for the precise construction of a complex geometry of cells and biologically active agents and is referred to as bioprinting[80]. Skeletal muscle TE in particular could benefit from the precise placement of cells, as structural organization is vital for muscle contraction and functionality[81]. In this work, we briefly note the benefits of scalability and efficiency 3D printing could have on skeletal muscle tissue engineering.

1.4.2 Physical topography of constructs

Scaffold topography can be purposely fashioned to provide guidance cues and to modulate cell response[82]. When considering methods for expediting the fusion of myoblasts into myofibers, we briefly looked into using scaffold topography to naturally align cells along grooves in collagen scaffolds.

1.5 Implantation strategies

Surgical implantation methods of skeletal muscle tissue engineered constructs are chosen to specifically emulate a particular disease or condition of relevance to human pathology. They range in invasiveness and scale, and some are better suited for modeling VML than others. Here we briefly discuss typical implantation models and why we selected our chosen model to study the performance of our TE skeletal construct *in vivo*.

1.5.1 Subcutaneous

Subcutaneous implantation is a simple surgical model placing a TE construct inferior to the skin but superior to the fascia of the muscle. This model is typically employed to evaluate whether the TE construct can undergo angiogenesis and survive *in vivo*. In a recent study, it was demonstrated that co-cultured endothelial cells and muscle progenitor cells (MPCs) seeded onto an ECM and implanted subcutaneously successfully formed vascularization *in vivo*[83,84]. This method has many benefits, but it has limited implications for studying VML injuries because it does not actually come in contact with skeletal muscle. Therefore, we searched for an alternative implantation strategy that directly impacted the injured muscle.

1.5.2 Dorsal skin fold window

Dorsal skin fold implants allow for real-time, non-destructive monitoring of implant survival and vascularization *in vivo*. In this model, the dorsal skin layer is removed to expose the subcutaneous tissue. Implants are laid in contact with the subcutaneous tissue and covered by a glass top and secured by a bioreactor that is sutured into the skin. Following treatment and observation, the implant and underlying skin can be explanted for ex vivo functional and histological assessment[32]. While this treatment can come into direct contact with skeletal muscle and is ideal when looking for minimally invasive treatment, it cannot effectively model or treat VML injuries. Therefore, we chose the most invasive but also most effective model; intramuscular implants.

1.5.3 Intramuscular

Intramuscular implants more closely model corrective surgery and aim to assess a TE construct's capacity to integrate with the hosts musculature or endogenous repair mechanisms in order to restore contractile function. This method is ideal for studying VML, as drastic procedures can remove 10%-20% of the muscle volume to mimic a large simultaneous loss of muscle, vasculature, and neurons seen in VML injuries. Implants are then used to fill the space left in the wake of large muscle volume loss and are monitored for long term integration and functional recovery *in vivo*[83] and *ex vivo*[85].

1.6 Hypothesis

The overriding hypothesis of this study was that second generation TEMR construct, or TEMR IIs, made possible by specialized bioreactor preconditioning, would yield significant long-term functional improvements after large VML injury in an immune competent rat model. To this end, VML injuries, with or without the implanted TEMR II technology, were examined in an established Rat LD VML injury model for their ability to enable restoration of function and native tissue morphology.

2. Chapter 2 - Advances in Biomanufacturing of TEMR Implants

Introduction

Ideal TE implants for VML wounds would be fully realized, genetically matched, mature, vascularized, innervated, and contractile skeletal muscle. Short of this technology, we aim to implant scaffolds that are seamlessly incorporated into the native tissue, triggering the body's endogenous repair mechanisms to reconstitute vascularized and contractile skeletal muscle fibers. It is critical to rebuild the body's native tissue if no donor tissue is readily available or the tissue damage is too extensive to allow for donor transplant.

The existing TEMR technology from our lab does an excellent job addressing this issue in immunocompromised mouse models, regenerating ~70% of functional capacity in skeletal muscle VML models when compared to uninjured controls. We see similar results in a rat TA study[76] and a later rat LD[31] study from our lab. A critical part of the success of this therapy is a cyclic mechanical stretch bioreactor that preconditions scaffolds to arrange myoblasts into myotubes. As previously discussed, however, there is evidence that a more densely seeded scaffold in a larger, immune competent model would more closely mimic the eventual target of this technology – humans.

Achieving a double seeded scaffold in the current bioreactor model is a tedious process that requires meticulous attention to detail, extremely precise fine motor skills, extensive amounts of time, and is difficult to distinguish between sides that have been double seeded without compromising the scaffolds by viewing them under a microscope. What we needed was a way expedite the process without compromising the cell layers. To do this, our team crafted the next generation bioreactor. David Remer did much of the software design, and together with my feedback about the ergonomic functionality and bioreactivity, we created a bioreactor that could address these hurdles with ease and elegance.

2.1 Novel Bioreactor

2.1.1 Specifications

The bioreactor is a CAD designed device milled from Teflon, nylon and acrylic designed to apply cyclic mechanical stretch to seeded BAMs, while maintaining aseptic and physiologically relevant conditions for MPCs. In the original iteration of the bioreactor, seeded BAMs are mounted with Teflon clamps in a fixed position and stretched using a computer-controlled stepper motor. The newer design (developed in collaboration with David Remer), and the focus of this thesis, mounts scaffolds to a removable Teflon frame (Fig. 1A-B) that sits within the bed of the bioreactor (Fig. 1D). The frame consists of two "bars" (Fig. 1A) and two "crossbars" (Fig. 1B) that are connected with adjustment slots that allow the bars to laterally translate such that distance between the bars can fluctuate by several centimeters. One side of the frame remains stationary via friction fit while the other is connected to a custom Haydon Kerk/Ametek (Waterbury, CT) linear stepper motor

that is mounted directly on the side of the bioreactor (Fig. 1, E). Everything is kept sterile with a custom-fit acrylic lid that has filtered, gas exchange holes (Fig. 1C).

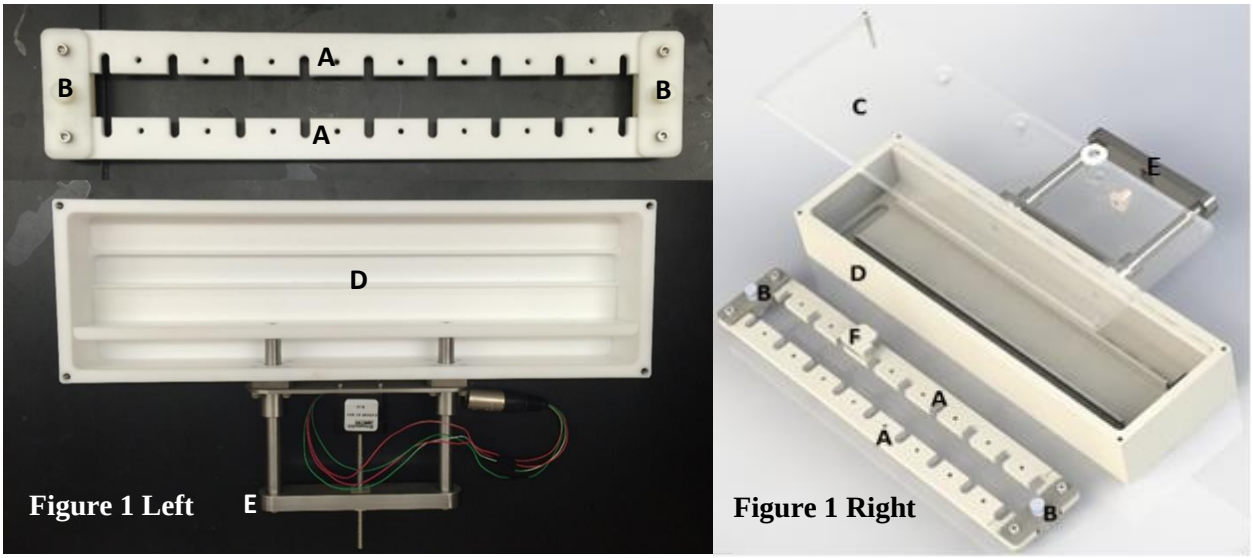

Fig 1. **Design of the bioreactor.** Illustrates improved design for bioreactor featuring an insertable apparatus for flipping scaffolds with minimal interference. These images depict a picture (left) and CAD drawing (right) of the insertable apparatus and its component parts as bars (A) and crossbars (B) resting outside of the bioreactor. The lid (C, not shown on left) is secured to the bioreactor body (D) via 4 corner screws. Metal struts (E) support a stepper motor (not pictured on the right) that applies cyclic mechanical stretch to scaffolds (not pictured here) held fast with clamps (F).

The bioreactor is capable of holding eight small scaffolds (1.2cm x 1.5cm) or three large scaffolds (2cm x 3cm) concurrently. Scaffolds are secured such that the bars are 3.0cm apart at rest (i.e. no stretch) (Fig. 2). Teflon clamps are aligned using nylon studs and are securely fastened with nylon thumbnuts. Scaffolds are sandwiched between the bar of the frame and the compression of the Teflon clamp, thus holding the scaffolds firmly in place. HeliCoils (Stanley Engineered Fastening, USA) are used to protect the soft Teflon body of the bioreactor at the screw interfaces found at the motor mount and in the body holes used to secure the lid.

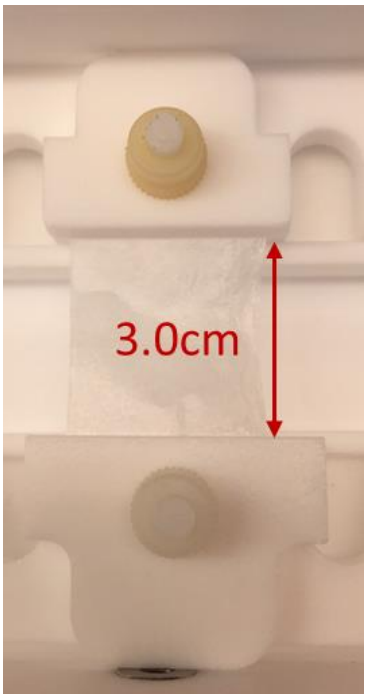

Fig 2. **Scaffolds clamped into the bioreactor.** Demonstrates the distance between clamps fastened in the novel bioreactor. The total distance is 3.0cm, and is measured with a sterile surgical ruler for each scaffold placed in a bioreactor.

Protocol

Previous work in our lab[6,31,72,76] developed a protocol for a cyclic mechanical stretch sequence that successfully aligned myoblasts along the axis of mechanical strain. The protocol begins with the immediate 10% stretch of the scaffolds' starting length, for a total

stretch distance of ~3mm. Stretch and retraction occurs over 10 seconds, with peak stretch occurring at 5 seconds and resuming original position at 10 seconds. This cycle is repeated three times a minute for the first five minutes of every hour, for a total of 15 repetitions every hour. The cycle is paused for 55 minutes and repeats the cycle. This protocol continues for 5 days.

2.1.2 Sterilization & Use

Sterility is critical to success in cell culture. Pieces of the bioreactor are disassembled, washed, bleached, and sterilized by ethylene oxide sterilization at 37C. When ready for use, sterilized components are brought into the hood and assembled aseptically, setting the lid aside until scaffolds can be placed in the bioreactor. The bioreactor chamber is then filled with proliferation media such that the media is flush with the lip of the bars. Using sterile forceps, seeded BAMs are positioned over the gap and one side is fastened with a Teflon clamp. Using forceps again, the second side of the seeded BAM is pulled taught and clamped (Fig. 2). When all BAMs are in place, the bioreactor is filled with proliferation media such that the scaffolds are fully immersed in fluid. The lid is then firmly fastened in place with 6 screws, and placed in an incubator. Cables connecting the stepper motor to the controller do not obstruct the integrity of the incubator seal. The controller is set to run the cyclic mechanical stretch protocol as previously described. After preconditioning, a seeded BAM is referred to as a TEMR.

Fig 3. **Novel Bioreactor frame during flip**. 6 scaffolds are attached and simultaneously being lifted out of the bioreactor to be flipped. All scaffold handling is done in a BSC hood with proper aseptic technique.

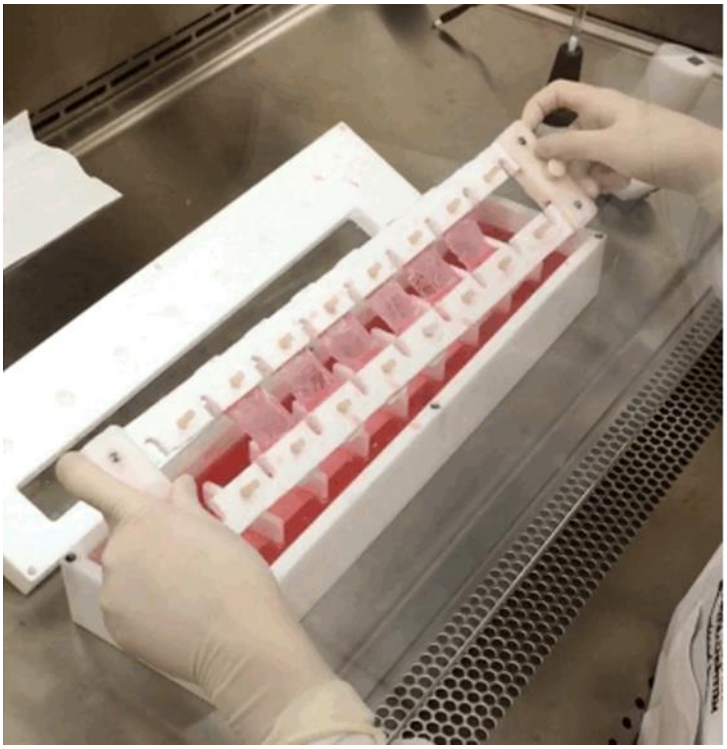

The removable and flippable frame is an integral part of the novel bioreactor design, without it the TEMR II technology would be nearly impossible to manufacture. As previously described, the scaffolds are held in place within the bioreactor using Teflon clamps. In the old bioreactor design that lacked the frame, each individual scaffold would have to be unclamped, lifted and flipped 180°, and re-clamped in the bioreactor. It would also be very difficult to distinguish between which scaffolds have been flipped, as there was no way to mark this action within the bioreactor. The novel frame does several actions. First, it serves as a minimally invasive tool to flip scaffolds such that any cell layers present on the scaffold will not be disturbed (no unclamping or fidgeting with scaffolds required). Second, it can flip multiple scaffolds simultaneously, dramatically reducing the time required to

manufacture TEMR IIs. Finally, the frame can be marked to easily identify scaffold sides.

Flipping the frame is a decidedly straightforward process. After placing the bioreactor in the hood and removing the lid, handles on the frame can be used to lift and flip the frame 180° along the long edge of one of the bars (Fig. 3). The lid is replaced, and scaffolds are left to statically incubate until they are ready to be flipped and stretched again.

2.1.3 Weaknesses

The bioreactor is a robust piece of equipment. There are, however, a few minor revisions that could be made to further optimize the use and ergonomic appeal of the system. Currently, when the frame is rotated 180° along the long edge of the bars, the clamps holding the scaffolds in place prevent a snug friction fit of the frame into the bioreactor. This leaves the frame slightly raised, and the bioreactor chamber requires more media to submerge the scaffolds at their slightly elevated position. Additionally, because the frame is not snug, the scaffolds cannot be stretched until the frame is again flipped 180° along the long edge of the bars back to its original position. This does not inhibit cell culture or the generation of TEMR IIs, but it does use considerably more media and significantly elevates the cost of production. Designs are currently being discussed to improve these issues.

2.2 Seeding

2.2.1 Cell Harvesting and Preparation

As previously discussed, the ultimate target of this technology are human patients. We needed a process that would mimic gathering cells for implantation in a human patient that has already experienced severe trauma. For our purposes, it made sense to take a small biopsy of muscle either from the wound bed during debridement or from another, minimally impacted muscle tissue. MPCs could be harvested from digested healthy tissue, mitigating implant rejection (as cells are directly from the host) and maximizing incorporation of the implant into the endogenous healthy tissue. With forward thinking, we chose to harvest MPCs from mature tissue for implantation into the wound bed.

MPCs for seeding BAMs were isolated from surgical biopsies of the tibialis anterior and soleus muscles of 4-6 week old male Lewis rats purchased from Charles River. Muscles were removed of tendon and fascia, and then sterilized in iodine and subsequent phosphate-buffered saline (PBS) washes. Sterilized muscles were transferred into a 0.2% w/v collagenase (Worthington Biochemical, Lakewood, NJ) low-glucose DMEM (Hyclone, USA) solution where they were finely minced by hand for 10 minutes and then allowed to further digest at 37°C for 2 hours. The muscle slurry was then plated onto tissue collagen coated culture dishes for 24hrs. Media was aspirated and moved to culture dishes coated with Matrigel (1:50 dilution; BD Biosciences) in myogenic media consisting of DMEM high glucose supplemented with 20% FBS, 10% horse serum, 1% chicken embryo extract, and 1% antibiotic/antimycotic (AA; Hyclone) and incubated at 37° for 72 hours. Media was then changed to seeding media consisting of low-glucose DMEM supplemented with 15% FBS and 1% AA. Cells were passaged at 70-80-% confluence.

2.2.2 Bladder Acellular Matrix Preparation

As stated, the BAMs are particularly useful in that they effectively serve as biomechanical, biochemical, and structural analogs to native ECM; they bridge large gaps in endogenous ECM and integrate into endogenous tissue with little or no rejection. Here we describe how we derive BAMs for TEMR fabrication.

BAM scaffolds were prepared from porcine urinary bladder as previously described[6,31,72,76]. Briefly, bladder was washed and trimmed to obtain lamina propria, which was then placed in 0.05% trypsin (Hyclone) for 1 h at 37°C. The bladder was then transferred to DMEM solution supplemented with 10% FBS and 1% AA and kept overnight at 4°C. The preparation was then washed in a solution containing 1% triton X (Sigma-Aldrich) and 0.1% ammonium hydroxide (Fisher Scientific) in de-ionized water for 4 days at 4°C. Finally, the bladder was then washed in de-ionized water for 3 days at 4°C. The decellularized scaffold was then peeled by hand with tweezers to obtain a scaffold of 0.2-0.4 mm thickness. The scaffolds were then cut and draped onto custom-made silicone molds with a 6 cm 2 working area (1.2cm x 1.5cm rectangle). Scaffolds and molds were placed in individual cell culture dishes and frozen at -20°C, then lyophilized. Lyophilized scaffolds were sterilized using ethylene oxide and stored in a dry, dark drawer until ready for use. At this point, BAMs are dry and brittle until rehydrated at later steps (Fig. 4). Side 1 was denoted as the side that "cupped" the silicone mold and side 2 was the reverse (Fig. 4 B,D).

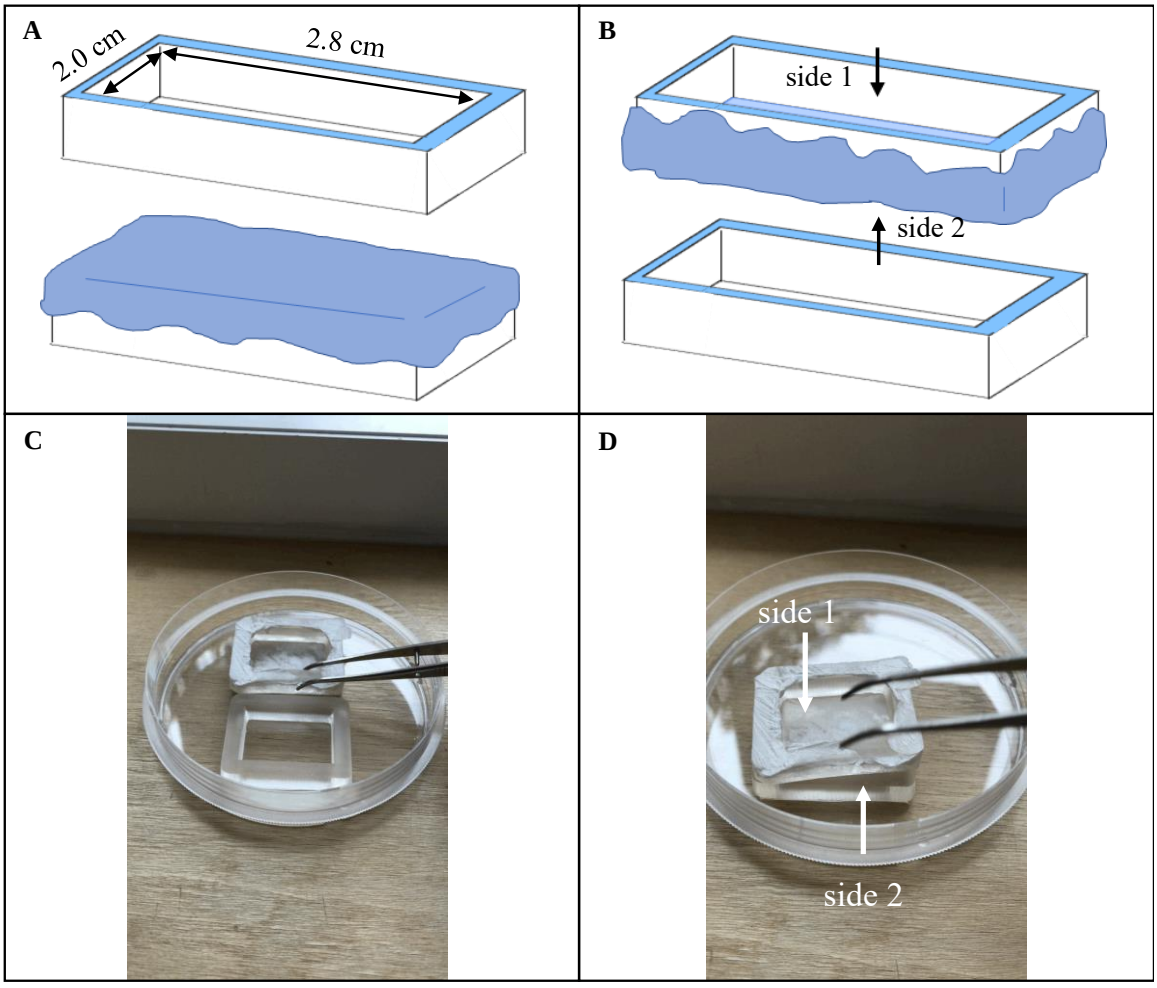

Fig 4. **Dehydrated BAM on silicone mold and sides of the BAM.** Here we can see a schematic (A and B) and picture (C and D) of dehydrated BAMs. As the BAMs lyophilize, they have a shrink-wrap effect on the mold (top A and bottom B) and adhere to the mold without any assistance of glue. Sides one and two are indicated in B and D.

2.2.3 TEMR protocol

The original regenerative technology developed in this lab was the Tissue Engineered Muscle Repair, or TEMR platform. This construct is the building block for the TEMR II, the focus of this thesis. Here we briefly discuss the process for generating TEMRs so we can later highlight the distinction between the TEMR and TEMR II development processes.

TEMR constructs were created from sterilized scaffolds that were immersed in seeding solution consisting of DMEM, 15% FBS, and 1% AA at 37°C for 10 minutes prior to cell seeding. This step restores the elasticity of the scaffolds and minimized risk of tearing during the seeding process. MPCs (passage 2) were then seeded at a concentration of 1 million cells per cm^2 on one side, designated as "side one", and after 24 h, the scaffolds were flipped, and cells were seeded at a concentration of 1 million cells per cm^2 on the other side, or "side two." Seeded scaffolds were incubated at 37°C for 48 hours before changing to differentiation media consisting of DMEM F:12 1:1 (Gibco). Differentiation media was changed every 72 hours for 6 days. On the sixth day of static culture, seeded BAM scaffolds were removed from the silicone molds using sterile forceps to me moved to bioreactors as described previously[6,76]. Scaffolds were securely held in place using clamps on each of the 1.2cm edges, being careful not to disturb the cell layer. Bioreactors were then filled with seeding solution such that scaffolds were completely submerged. Cyclic mechanical stretch protocol was initiated as described above.

2.2.4 TEMR II protocol

Initial steps and cell culture for fabricating the TEMR II are identical to TEMR construct generation. BAMs are hydrated, seeded at 1 million cells per cm^2 on both side one and two, given 48 hours to proliferate before switching to differentiation media, grown in differentiation media for 6 days, and finally placed in the bioreactor for cyclic mechanical stretching. On day three of mechanical stretching in the bioreactors, stretching is paused for re-seeding the constructs. MPCs (passage 3-4) are then seeded at a concentration of 1 million cells per cm^2 on side one. After 6h of static incubation at 37°C, the constructs are simultaneously flipped by gently lifting removable bars from the bioreactor, flipping the constructs and bars by 180° along the long edge of the bar (Fig. 3), and placed back into the bioreactor. Cells are then seeded at a concentration of 1 million cells per cm^2 on side two. At this point, the constructs are referred to as "double seeded" because each side has received a total of 2 million cells per cm^2 over two different seeding periods. Double seeded constructs are incubated at 37°C for 6 hours before flipping the constructs and bars 180° again such that side one is facing up, and resuming cyclic mechanical stretching. Stretching proceeded as described above for 2 more days. The implications for this densely seeded constructs will be thoroughly discussed in section 3.

2.3 Quantification

2.3.1 Acquiring Samples

It is critical to establish that double seeding the construct does, in fact, morphologically distinguish TEMR II from TEMR constructs. It is possible that the second seeding may have no effect or even deleterious effects on cell density, myofiber alignment, and viability of cells, thus it is critical to histologically determine benefits of the TEMR II technology. To this end, we regularly imaged

one TEMR II from every batch of TEMR II production that were to be implanted as a quality control measure. Here, we describe the procedures used to perform this quality control check.

Histological procedures for TEMR and TEMR II are identical. Following cyclic mechanical stretch, the bioreactor was placed in the biosafety cabinet hood and constructs to be stained were removed from the bioreactor using sterile forceps and set into sterile 5cm petri dishes.

2.3.2 Staining

Whole-mount staining was performed by fixing the cells in 4% paraformaldehyde, washing in phosphate-buffered saline (PBS)-glycine (10mM), permeabilizing with 0.5% triton, and then washing again in PBS-glycine. Scaffolds were then trimmed and cut in half. The halves were mounted on a polarized glass slide such that each side of the scaffold was touching the coverslip, then bordered with a hydrophobic marker. Cells were then blocked in Dako Protein Block (Aligent, CA) for 30 minutes at room temperature prior to incubation with primary antibodies raised in chicken against phalloidin-Alexa Fluor 488 or 594 conjugated (1:500 dilution, Invitrogen). Cells were then washed again, and probed specimens were coverslipped with VectaShield including DAPI.

2.3.3 Imaging

All immunofluorescence (IF) images were taken on a Leica confocal microscope. Scaffolds were imaged 5 times on each side for a total of 10 times per scaffold. One image was taken from each quadrant of the side, and one image was taken directly in the center of the side (Fig. 5).

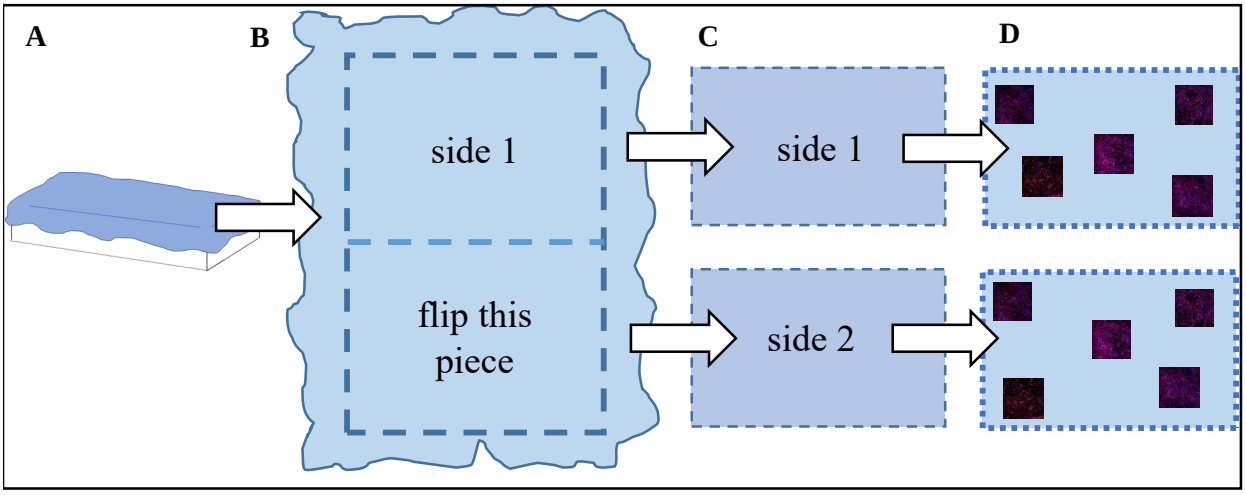

Fig 5. **Schematic of how scaffolds are imaged.** The seeded scaffold (A) is carefully removed from the mold and laid flat (B). Scaffolds are cut along the dotted lines such that there are two pieces of scaffold to image (C). One piece is flipped 180˚ along the short edge so that when both pieces are placed on a slide, both side 1 and side 2 will face the optical lens. Each side is imaged 5 times (D), once in each quadrant and once in the center of the scaffold.

2.3.4 Processing

All images were then read into MATLAB as a greyscale image for processing and cell counting. Red, blue, and green channels were separated, and the blue channel for each image was used for further processing. The blue channel was treated using the contrast-limited adaptive histogram equalization (CLAHE) adapthisteq function which enhances the contrast of grayscale images[86] . Treated images were then subsequently adjusted with the imclearborder function, which suppresses signal in the image that are lighter than their surroundings and connected to the image border, effectively distinguishing the perimeter of the individual cells[87].
The wiener2 filter was then used to reduce Gaussian noise[88]. All pixels were converted to binary using the im2bw function[89], then the imfill function was used to fill holes in the binary image[90]. Any pixels having a radius less than 2 were removed using the imopen function[91]. Further removal of noise was done by using bwareopen function to remove any connected pixel group with a radius less than 5[92]. Remainder of pixels were counted and exported to an excel file. Number of pixels were used as an approximation of total cells present, where more pixels represented greater cell signal, and thus indicated more cells present. All pixel counts from both sides of TEMR I (n=4) and TEMR II (n=8) scaffolds were compared to determine whether TEMR II technology yielded greater cell density.

2.3.5 Code

The following code was written to efficiently manage all immunofluorescent images for both TEMR I and TEMR II. The details of each of the functions used are described in the *Processing* section.

```
%read all images in a folder and execute
myFolder = 'C:\Users\kcs9ay\Desktop\MATLAB\4091-37\good';    % Specify the folder where the
files live.
contents = dir([myFolder '\*.jpg']);
nfiles = length(contents);
for i = 1:nfiles
   filename = contents(i).name;
   currentImage = imread(filename);
   [path name] = fileparts(filename); %open file specified in filename, do the processing
   img = currentImage;
% img = imread('4091-37.lif_bad_phal594_desmin488_dapi_10x_4_1Snapshot1_ch00.jpg');

% Read image
red = img(:,:,1); % Red channel
green = img(:,:,2); % Green channel
blue = img(:,:,3); % Blue channel
blue2 = adapthisteq(blue);  %adjust contrast of blue channel
blue3 = imclearborder(blue2); %cleans up perimeter of nuclei
blue4 = wiener2(blue3); %small window filter on image
blue5 = im2bw(blue4, graythresh(blue4));
blue6 = imfill(blue5, 'holes'); %fills holes in the nuclei
blue7 = imopen(blue6, strel('disk',2)); %morphologically opens using disk kernel
blue8 = bwareaopen(blue7, 5); %removes pixels of 'n' or less
totalpixelcount(i) = numel(blue8);
```

```
whitepixelcount(i) = sum(blue8(:));
blackpixelcount(i) = totalpixelcount(i) - whitepixelcount(i);

%export data to excel file
xlswrite('PositiveSignal4091-37good.xlsx', whitepixelcount)
xlswrite('NegativeSignal4091-37good.xlsx', blackpixelcount)
xlswrite('TotalSignal4091-37good.xlsx', totalpixelcount)

%figures
figure
subplot (3,3,1); imshow(img); title('Original Image');
subplot(3, 3, 2);imshow(blue);title('Blue Channel');
subplot(3, 3, 3);imshow(blue2);title('Adjusted Contrast');
subplot(3, 3, 4);imshow(blue3);title('Perimeter Clean');
subplot(3, 3, 5);imshow(blue4);title('Weiner Filter');
subplot(3, 3, 6);imshow(blue5);title('Binary Image');
subplot(3, 3, 7);imshow(blue6);title('Fill Holes');
subplot(3, 3, 8);imshow(blue7);title('Clear Background');
subplot(3, 3, 9);imshow(blue8);title('Remove Noise');
ha = axes('Position',[0 0 1 1],'Xlim',[0 1],'Ylim',[0 1],'Box','off','Visible','off','Units','normalized',
'clipping' , 'off');
text(0.5, 1, sprintf('\b 4091-37 good %i \n',i),'HorizontalAlignment','center','VerticalAlignment',
'top')
end
```

2.3.6 TEMR vs TEMR II Seeded scaffolds

As mentioned, the culmination of this histological analysis is to determine whether the double seeding procedure has any, positive or negative, effect on the TEMR technology. The TEMRs that were imaged were generated in a previous study (collaboration with Ellen Mintz), fixed, stained, and imaged according to the procedures outlined above. A total of 4 TEMR scaffolds were analyzed. Similarly, the TEMR II scaffolds were fixed, stained, and imaged. 8 total TEMR II scaffolds were analyzed. Images were qualitatively (Fig. 6) and quantitatively (Fig. 7) compared to assess cell density, homogeneity of cell coverage, and cell alignment.

Qualitatively, both sides of the TEMR and TEMR II seem comparable in cell alignment and density. There appears to be improved density on side two of TEMR II when compared directly to TEMR (Fig. 6). Quantitative analyses needed to be done to determine whether this perceived difference was indeed significant. The data generated from the MATLAB code show that while there is no significant ($p<0.05$) difference in cell density between side one of the TEMR vs TEMR II, there is indeed a significant difference on side two as was perceived by IF imaging.

This was exciting confirmation that double seeding did, in fact, yield greater cell density and ultimately an increased density of preconditioned, aligned progenitor muscle cells delivered to the wound bed.

Using this information and the hypothesis that increased cell delivery would have an effect on therapeutic outcomes of TE implants, we decided it was time to determine whether increased cell

delivery to the wound bed elicited improved functional and cosmetic outcomes to a VML model.

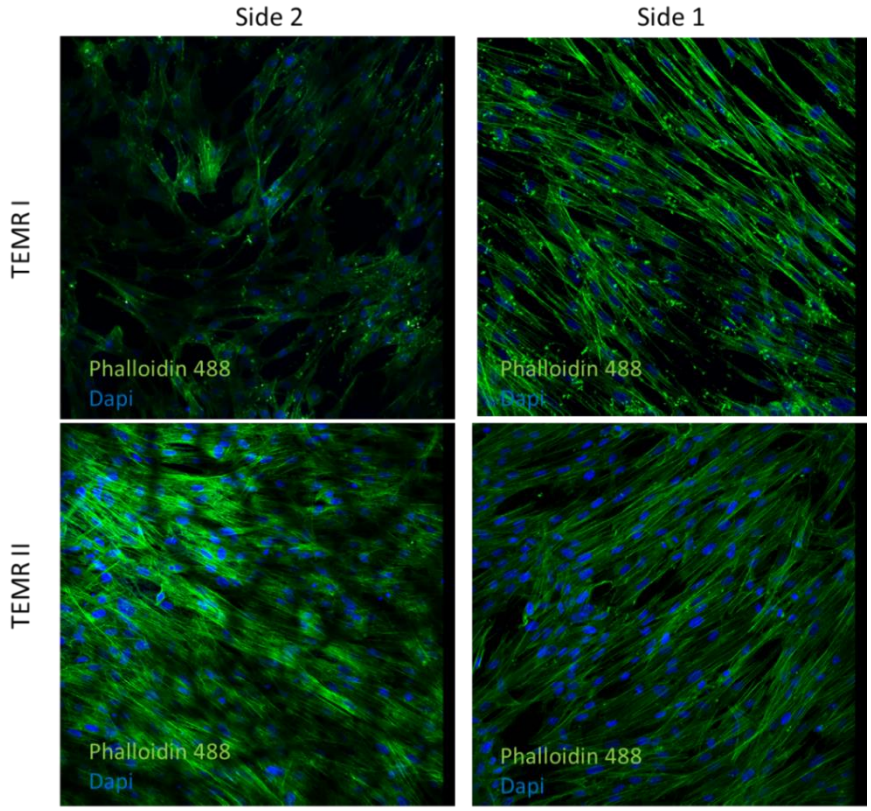

Fig. 6. **TEMR II has qualitatively superior coverage on side 2 of the scaffold when compared to TEMR I technology.** Here we see the improved homogeneity of seeding density on both sides of TEMR II versus TEMR using representative images from both groups. F-actin stained with phalloidin 488, cell nuclei stained with DAPI. At least 5 high-powered images (400x) were taken from each side of a scaffold. 4 total TEMR I constructs and 8 total TEMR II constructs were imaged.

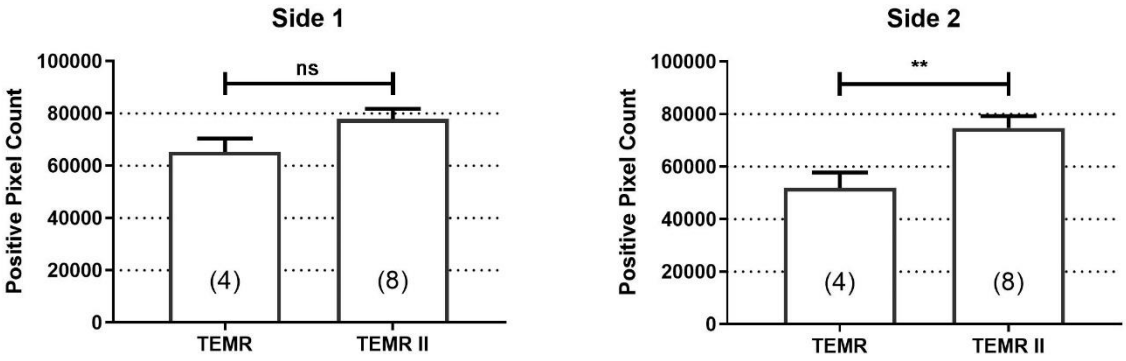

Fig 7. **TEMR II has quantitatively superior cell density when compared to TEMR I technology.** Blue pixels were counted in MATLAB and represented density of cells. We intentionally did not attempt to assign an average pixel count/cell because of the possibility of stacked layers of cells. According to these data, TEMR II side 2 has significantly ($p < 0.01$) more pixels representative of cells when compared to TEMR I constructs, while there is no difference (ns) on Side 1. Significance is noted by * ($p<0.05$), ** ($p<0.01$), and ns (not significant). Data were compared with unpaired t test.

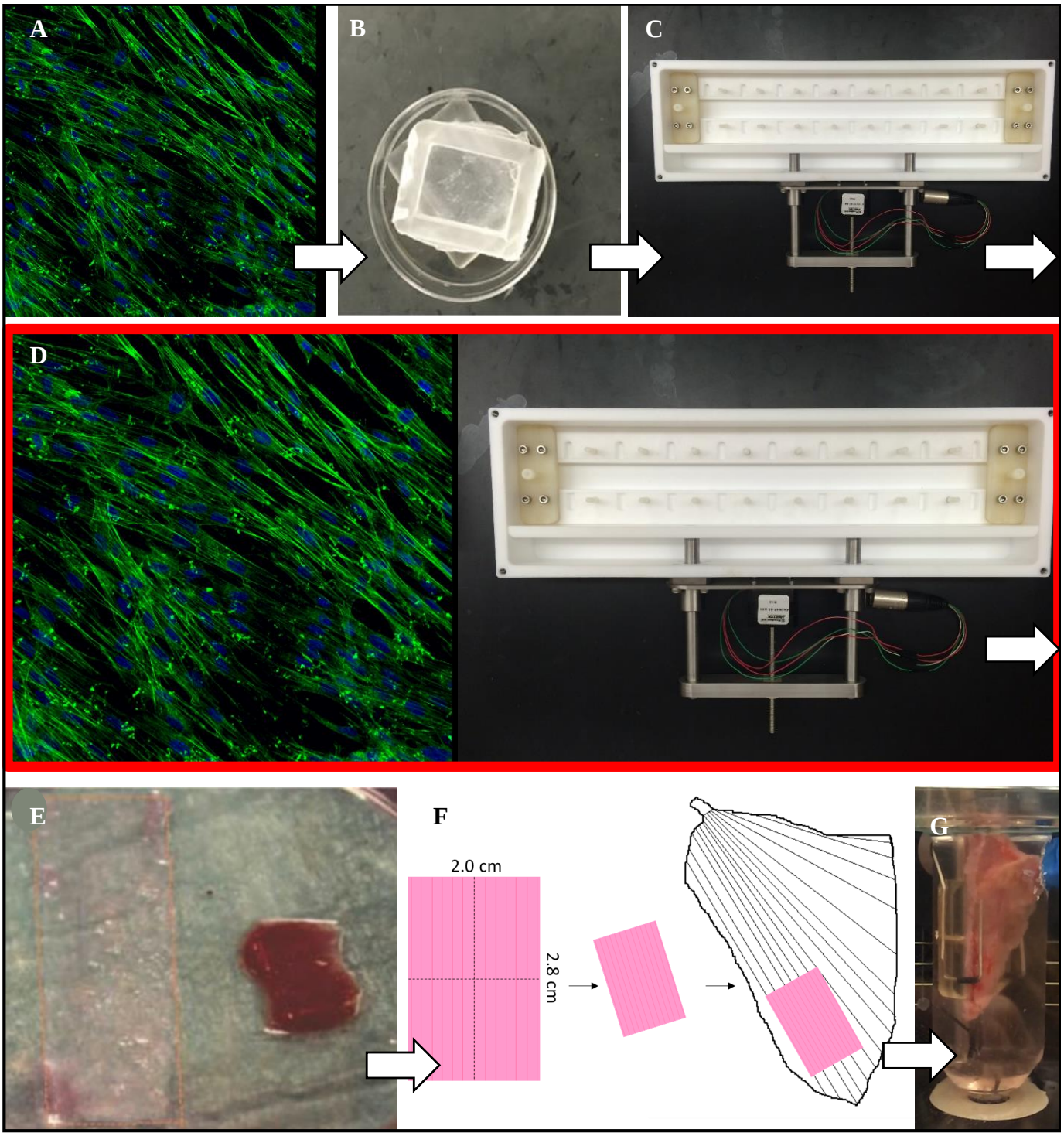

Fig 8. **Flow of TEMR II from seeding to implantation and functional testing.** (A) shows a confocal image of cells where blue is DAPI-stained nuclei and green is Alexa phalloidin 488-stained F-actin. (This particular image shows cells already seeded on a scaffold and is for conceptualization purposes only. It does not represent MPCs on a cell culture plate). Cells are then seeded onto prepared BAMs (B) and differentiated in static culture for several days. Seeded BAMs are then inserted into a bioreactor (C) for three days. On the third day, seeding is stopped and more cells are added (D, right), and stretching is resumed (D, left). Following the mechanical stretching protocol, constructs are identified as TEMRs and removed for trimming and folding (E, modified from a paper, and F). Folded constructs are placed inside of a wound created on the LD. Post treatment, muscles are excised and tested for mechanical output (G).

3. Chapter 3 - Evaluation of Functional Recovery Following In Vivo Implantation

Introduction

Patients who suffer from VML experience persistent functional deficits that, as one could imagine, reduce quality of life. Range of motion, total skeletal muscle force production, and endurance are all significantly impacted when large "chunks" of muscles are injured or missing. Even small increases in functional recovery could have major positive impact on patients; a minor improvement could mean the difference between near immobility of the affected limb and the ability to lift an arm to feed yourself.

It is our aim to create a skeletal muscle construct that not only mimics skeletal muscle morphology in vitro, but also restores the functional capacity in injured tissue to comparable functional capacities of native tissue in vivo. Our eventual human target for this technology is the adductor pollcis in the human hand. The adductor pollcis muscle is a thin, pinnated muscle that represented a humble starting ground for human clinical trials. If this technology would work in a small, thin muscle such as the adductor pollcis, it is reasonable to investigate this technology for longer, thicker muscles. The rat latissimus dorsi (LD) exhibits a similar pinnation pattern and comparable size to that of an adult human hand, and thus made for an excellent model.

To determine whether our construct restores functional capacity in the rat model, we must first make an injury. Our studies aimed to damage ~20% of the target skeletal muscle, and half of the damaged muscles were treated with our technology. Injured, treated, and control muscles were all tested for maximum force production output and compared. Here we discuss the specifics of the rat LD VML model and how functional recovery was tested.

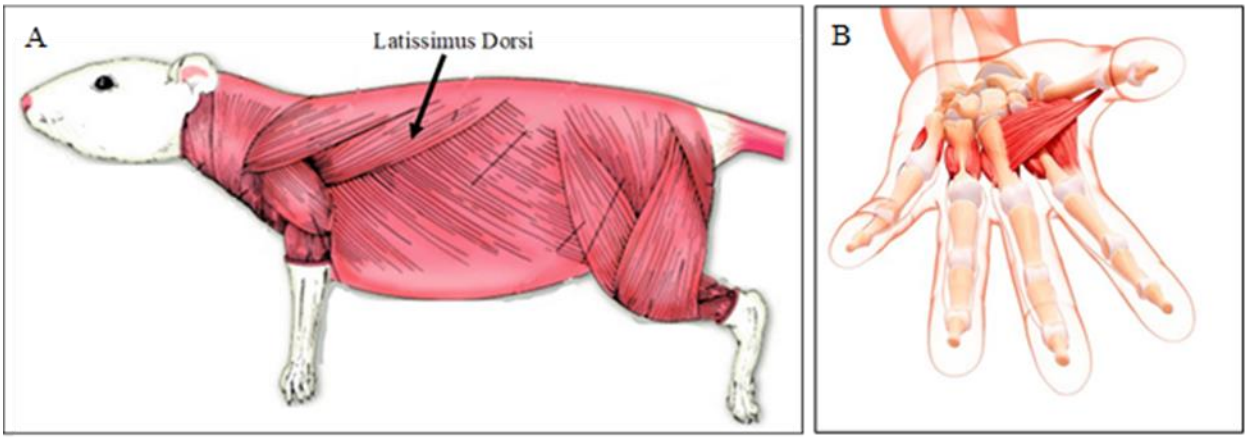

Fig 9. **Lateral view of Latissimus Dorsi on a rat and adductor pollcis in human hand.** (A) Shows the LD lying deep to the spinotrapezius and superficial to the external obliques. Image credit to Quizlet, minorly edited to erase distracting lines and labels[95]. (B) Schematic of adductor pollcis in human adult left hand with a transverse head originating from the third metacarpal and as oblique head on the capitate bone. Together these heads insert on the base of the proximal phalanx of the thumb[78].

3.1 LD VML model

3.1.1 Treatment groups and Experimental setup

This study directly compared TEMR II treated VML wounds to VML injury animals with no treatment. All treatments were compared to native, non-injured control muscles in adult male rats. All injuries were created on the left latissimus dorsi while the right latissimus dorsi were used as the uninjured control. Treatment groups and group sizes are listed in Table 1 and are as follows: no repair (NR) 2 months *n=8*, NR 4 months *n=8*, NR 6 months *n=8*, treatment with TEMR II 2 months *n=8*, TEMR II 4 months *n=12*, TEMR II 6 months *n=8*. Scaffolds were prepared as described previously.

Table 1. Summary of Treatment Groups in the Rat Latissimus Dorsi TEMR II Study

Treatment groups	*Time between surgery and explant*	*group size*	Components	
			VML Injury	*TEMR II Implant*
NR 2mo	2 months	8	+	-
NR 4mo	4 months	8	+	-
NR 6mo	6 months	8	+	-
TEMR II 2mo	2 months	8	+	+
TEMR II 4mo	4 months	11	+	+
TEMR II 6mo	6 months	8	+	+

Here we can see the names of each treatment group, the time after VML surgery to explant, the number of animals in each group, and whether a TEMR II construct was sewn in at the time of surgery.

3.1.2 Rat LD VML injury model

This study was conducted in compliance with the Animal Welfare Act, the Implementing Animal Welfare Regulations, and in accordance with the principles of the Guide for the Care and Use of Laboratory Animals. The University of Virginia approved all animal procedures. All animals were individually housed in a vivarium accredited by the American Association for the Accreditation of Laboratory Animal Care, and they were provided with food and water *ad libitum.*

We created the injury model in male rats from Charles River aged to 12 weeks ± 3 days. To begin preparation for surgery, animals were anesthetized using 2.0% isoflurane gas. Animals were then moved to a warm surgery table where 2% isoflurane gas was pumped through a nose cone. We removed the hair from the surgical area with electric clippers and then thoroughly cleaned the area with three successive wipes of alcohol and isopropanol. All surgical equipment was properly sterilized with steam or ethylene oxide.

We acknowledge the incredible heterogeneity in animal models, and took every precaution to mitigate the variables between experiments. We used several landmarks to create the VML injury as identically as possible in each animal. The initial 4 cm incision was created using a sterile scalpel approximately 4 mm to the left of the animal's spine and approximately 6 mm distal from the

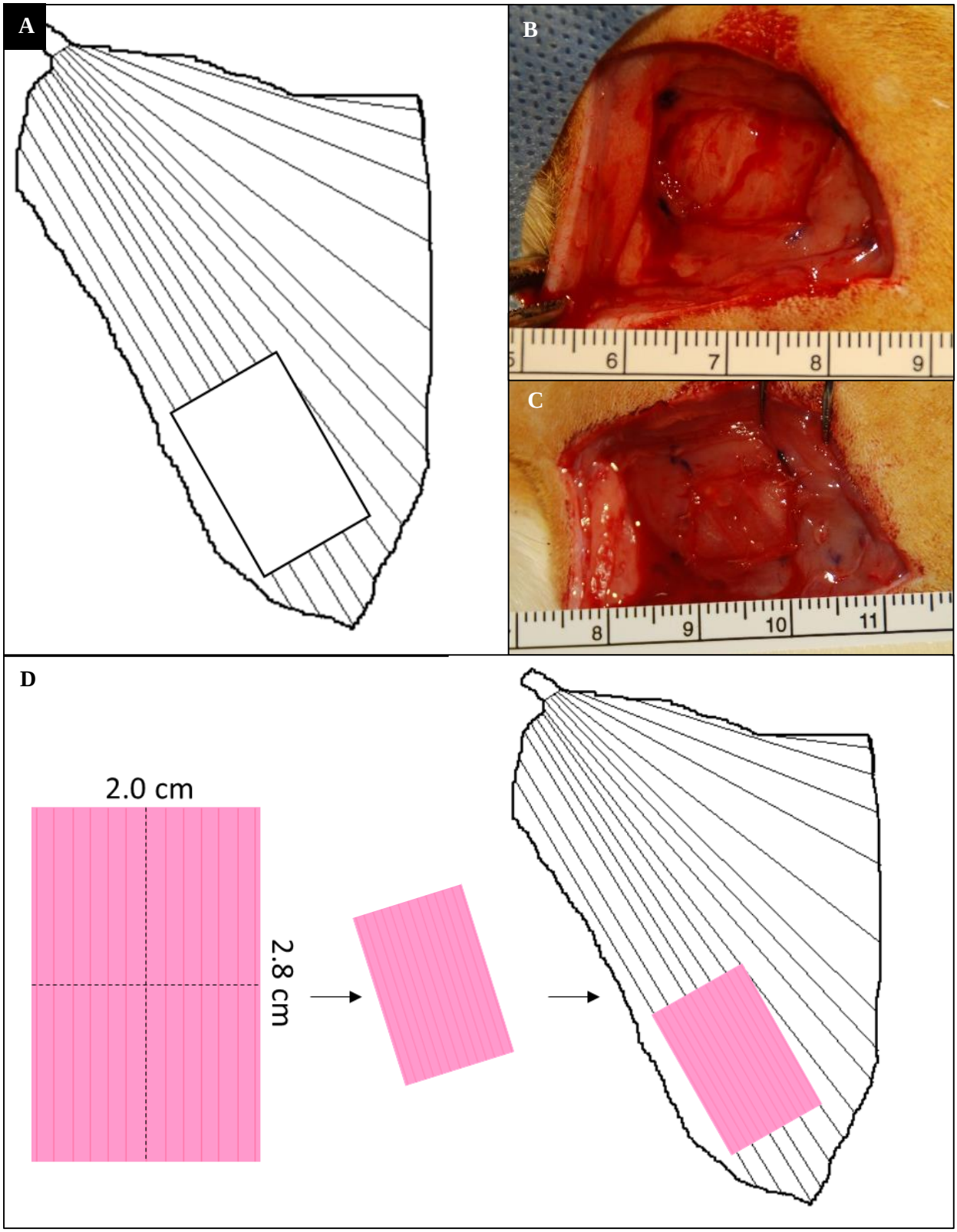

Fig 10. **The VML surgery and implantation of the TEMR II construct.** (A) is a pictogram that identifies the wound area cut out of the LD muscle. (B) Shows the surgically created VML wound in a rat, and (C) shows the TEMR II sewn directly into the surgically created VML injury. The process for folding the TEMR II construct prior to implantation is shown in (D).

armpit. We made a full-thickness cut that fully exposed the fascia of the muscle below. Using sterile micro scissors, we cut through the fascia and exposed the muscle below. At this location you could see the LD lying deep to the spinotrapezius. We then carefully separated the spinotrapezius from the LD using forceps, micro scissors, and sterile cotton swabs as needed. From there, we identified the bottom of the ribs by feel using the blunt end of a sterile cotton swabs. We measured 0.5cm distal from the base of the rib and approximately 1cm from the lateral edge of the LD to make the first mark using a surgical marker. Using this dot as reference, we made a rectangle of dots that measured 1.2 cm x 1.5 cm (Fig. 10). We then used sterile microscissors to gently cut out the rectangle of muscle. The excised muscle was weighed and disposed of in a biohazard bin. A camera and a surgical ruler were used to take a picture of each injury made. At this point, No Repair models were closed with simple interrupted sutures of the fascia and skin with sterile 6-0 vicryl and 4-0 prolene respectively. We covered the sutures in tissue glue to reduce unintentional suture removal. In TEMR II models, however, TEMR II construct was implanted as described below.

3.1.3 TEMR II Implant

TEMR II implant surgeries were scheduled to coincide with the same day TEMR II constructs are ready for implantation. Therefore, TEMR II constructs are housed in sterile conditions in the bioreactor at 37°C until the surgical VML wound has been made. At this point, TEMR II constructs are aseptically removed from the bioreactor and delivered to the surgeon. The surgeon then removes any excess scaffolding on the TEMR II construct using a sterile scalpel and folded as shown in Fig. 10D. Great care is taken to minimally disturb the cell layers on the TEMR II construct during folding and implantation. The four corners of the folded constructs are gently sutured into the four corners of the surgical wound. Four additional sutures are added at the midpoint of each side of the folded construct, for a total of eight sutures. As was the case with No Repair models, TEMR II models were then closed with simple interrupted sutures of the fascia and skin with sterile 6-0 vicryl and 4-0 prolene respectively. We covered the sutures in tissue glue to reduce unintentional suture removal.

3.1.4 Post-operative care

All animals were housed individually and monitored daily post-surgery. Immediately following surgery and every other day thereafter for a total of 5 days all animals were administered a subcutaneous shot of Slow Release Buprenorphine dosed according to the animals' individual weights to mitigate surgery associated pain. Open wounds were infrequent in LD models, but if any occurred wounds were promptly cleaned and re-sutured using 4-0 prolene and tissue glue. If any re-suturing was done following the initial VML injury surgery, the 5 days of individual housing and SR dosing were repeated. If no issues occurred after the first 5 days of monitoring, animals were paired in cages for socialization.

3.2 Ex vivo functional testing

3.2.1 Muscle excision

To begin preparation for surgery, animals were anesthetized in a gas-tight chamber with 2.0% isoflurane gas. Animals were then moved to a warm surgery table where 2% isoflurane gas was

pumped through a nose cone. We removed the hair from the surgical area with electric clippers and then removed any excess hair from the area using masking tape. An approximately 6cm full-thickness incision was made just to the left of the spine using a sterile scalpel. We then cut through the fascia and then bluntly separated it from the underlying muscles using cotton swabs. The entire LD muscle of each rat was isolated from the thoracolumbar fascia to the humeral tendon and the tendon and facial ends were tied with 5-0 silk suture (Fig. 11A). We transferred the muscle to Krebs-Ringer buffer solution (Sigma; composition: pH 7.4; concentration in mM: 121.0 NaCl, 5.0 KCl, 0.5 MgCl2, 1.8 CaCl2, 24.0 NaHCO3, 0.4NaH2PO4, and 5.5 glucose) in an Organ DMT system (Fig. 11B).

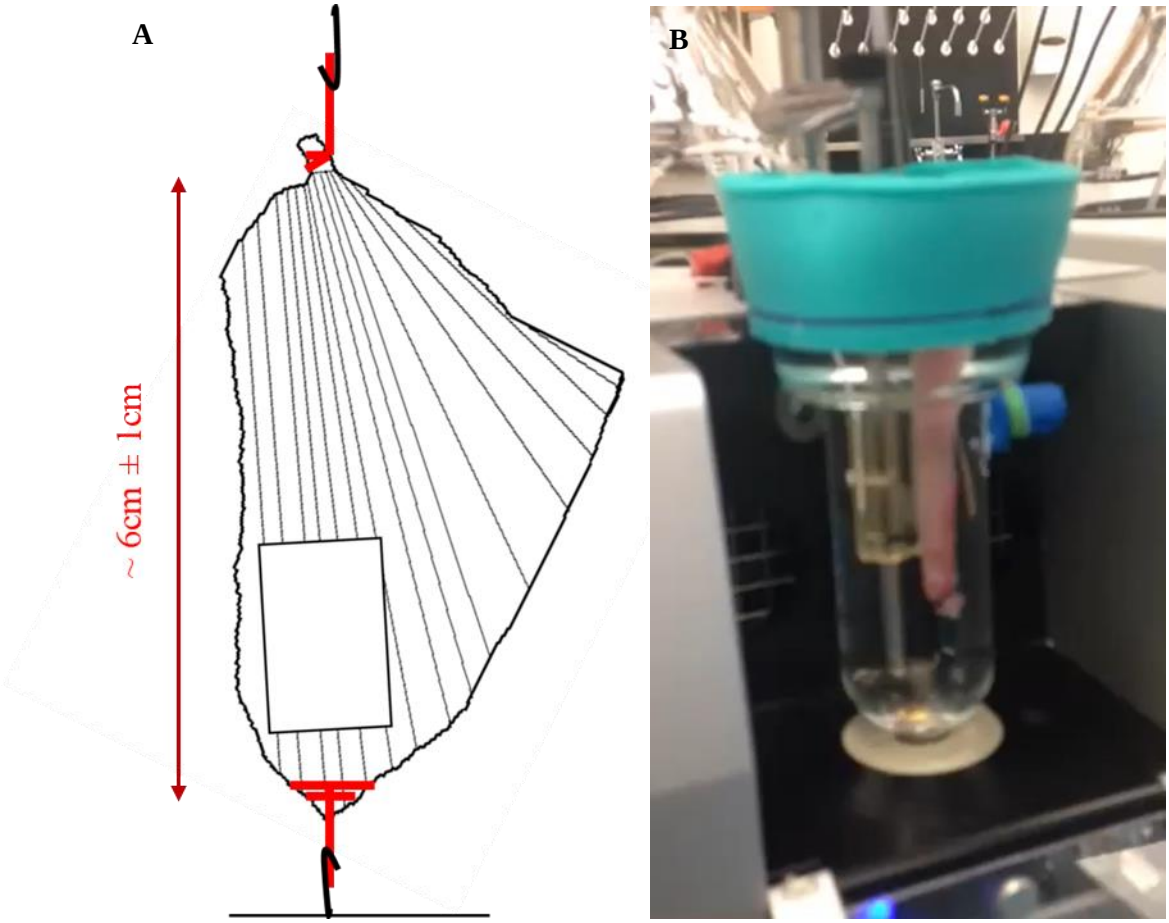

Fig 11. **Setup of explanted LD muscles in the DMT organ bath to measure force production.** The LD muscle is tied at the tendon and around the base of the muscle (shown in red in A) and attached to hooks present in the custom DMT organ bath. An actual picture of a muscle in the DMT organ bath is shown in (B).

3.2.2 DMT protocol

Muscles were transferred to individual chambers of a DMT 750 tissue organ bath system (DMT, Ann Arbor, MI) filled with Krebs-Ringer buffer at 35C bubbled with 95% O_2 and 5% CO_2. The

muscles were positioned between custom made platinum electrodes with the proximal tendon attached to a force transducer and the distal tendon to a fixed support. LD muscles were allowed to equilibrate for 5 minutes before determining optimal physiological muscle length (Lo) through a series of twitch contractions. We applied direct muscle electrical stimulation (0.2 ms pulse at 30V) across the LD muscle using a Grass 288 stimulator (Grass, Warwick, RI). We measured force as a function of stimulation frequency (1-250 Hz) at 37C during isometric contractions (750 ms trains of 0.2ms pulses), with 2 minutes between contractions. Real-time display and recording of all force measurements were performed on a PC with Power Lab/8sp (AD Instruments, Colorado Springs, CO). Of note, tissues that were inadvertently damages during retrieval or testing were not included in the contraction measurement data.

3.3 Force Production Results

3.3.1 VML Injury

Table 2 lists the average VML injury sizes created for each group (refer to Table 1). All injuries were created as described above.

Table 2. Summary of Rat Latissimus Dorsi VML Injury Creation Data in Male Lewis Rat

Treatment groups	*NR*	*TEMR II*
2 months		
sample size, *n*	8	8
defect weight, g	0.14 ± 0.01	0.12 ± 0.01
theoretical LD weight, g	1.05 ± 0.07	1.06 ± 0.05
% defect	14.70 ± 2.21	9.08 ± 2.00
4 months		
sample size, *n*	8	12
defect weight, g	0.12 ± 0.01	0.14 ± 0.01
theoretical LD weight, g	1.07 ± 0.05	1.12 ± 0.03
% defect	11.54 ± 0.74	12.36 ± 0.23
6 months		
sample size, *n*	8	8
defect weight, g	0.17 ± 0.01	0.16 ± 0.01
theoretical LD weight, g	1.29 ± 0.05	1.14 ± 0.03
% defect	13.17 ± 0.69	14.64 ± 0.80

Values are expressed as mean ± standard error of the mean. Theoretical LD weight is an approximation and is calculated by the following equation: (body weight of the animal x 0.37) / 100. Percent defect estimates the total percentage of LD tissue that is removed and is calculated by (defect weight / theoretical LD weight) x 100.

Table 3. Summary of Force-Frequency Measurements of Rat Latissimus Dorsi at 2, 4, and 6 Months Post TEMR II Implantation

Treatment groups	*Contralateral control*	*NR*	*TEMR II*
2 months			
sample size, *n*	16	8	8
50 Hz	1119.0 ± 69.6^{a}	305.8 ± 61.6^{b}	520.8 ± 38.7^{b}
100 Hz	2833.9 ± 156.2^{a}	1044.3 ± 322.6^{b}	1879.4 ± 126.7^{c}
150 Hz	3031.8 ± 170.6^{a}	1411.6 ± 335.0^{b}	2070.1 ± 152.1^{c}
250 Hz	2970.0 ± 160.0^{a}	1362.8 ± 334.0^{b}	1981.3 ± 152.5^{c}
4 months			
sample size, *n*	20*	8	12*
50 Hz	834.1 ± 38.7^{a}	389.3 ± 74.2^{b}	464.2 ± 59.4^{b}
100 Hz	2473.0 ± 117.6^{a}	1154.9 ± 132.5^{b}	1518.6 ± 203.9^{b}
150 Hz	2887.0 ± 156.8^{a}	1244.1 ± 134.2^{b}	1877.8 ± 235.2^{b}
250 Hz	2854.8 ± 159.7^{a}	1038.5 ± 131.8^{b}	1817.0 ± 247.1^{c}
6 months			
sample size, *n*	16	8	8
50 Hz	922.2 ± 84.0^{a}	265.3 ± 56.8^{b}	467.1 ± 37.6^{c}
100 Hz	2606.7 ± 186.2^{a}	940.5 ± 76.4^{b}	1725.5 ± 108.3^{c}
150 Hz	2938.6 ± 143.7^{a}	985.6 ± 92.5^{b}	1958.2 ± 128.2^{c}
250 Hz	2702.9 ± 174.0^{a}	826.1 ± 103.6^{b}	1840.2 ± 155.4^{c}

Values are expressed as mean ± standard error of the mean. Values denoted with the same letter across rows are not significantly different ($p > 0.05$), while values without a like letter denotation across rows are significantly different ($p < 0.05$). *one animal died during explanation and thus this sample size is *n*-1 compared to Table 2.

3.3.2 Statistics

Numeric data are presented as mean ± standard error of the means (SEM). Functional data were statistically analyzed by ordinary one-way ANOVA to compare mean differences between groups (Control, TEMR II, and NR). When significance was found ($p<0.05$), a post hoc multiple comparison test was used to compare group means ($p<0.05$) using a Fisher least significant difference (LSD) significance test. Statistical analyses were conducted using GraphPad Prism 6.0 for Windows.

3.3.3 Isometric Force Production

Our data was collected in two ways: First, we measured and calculated the average isometric force production as a function of stimulation frequency for each group (as defined in Table 1) at 50, 100,

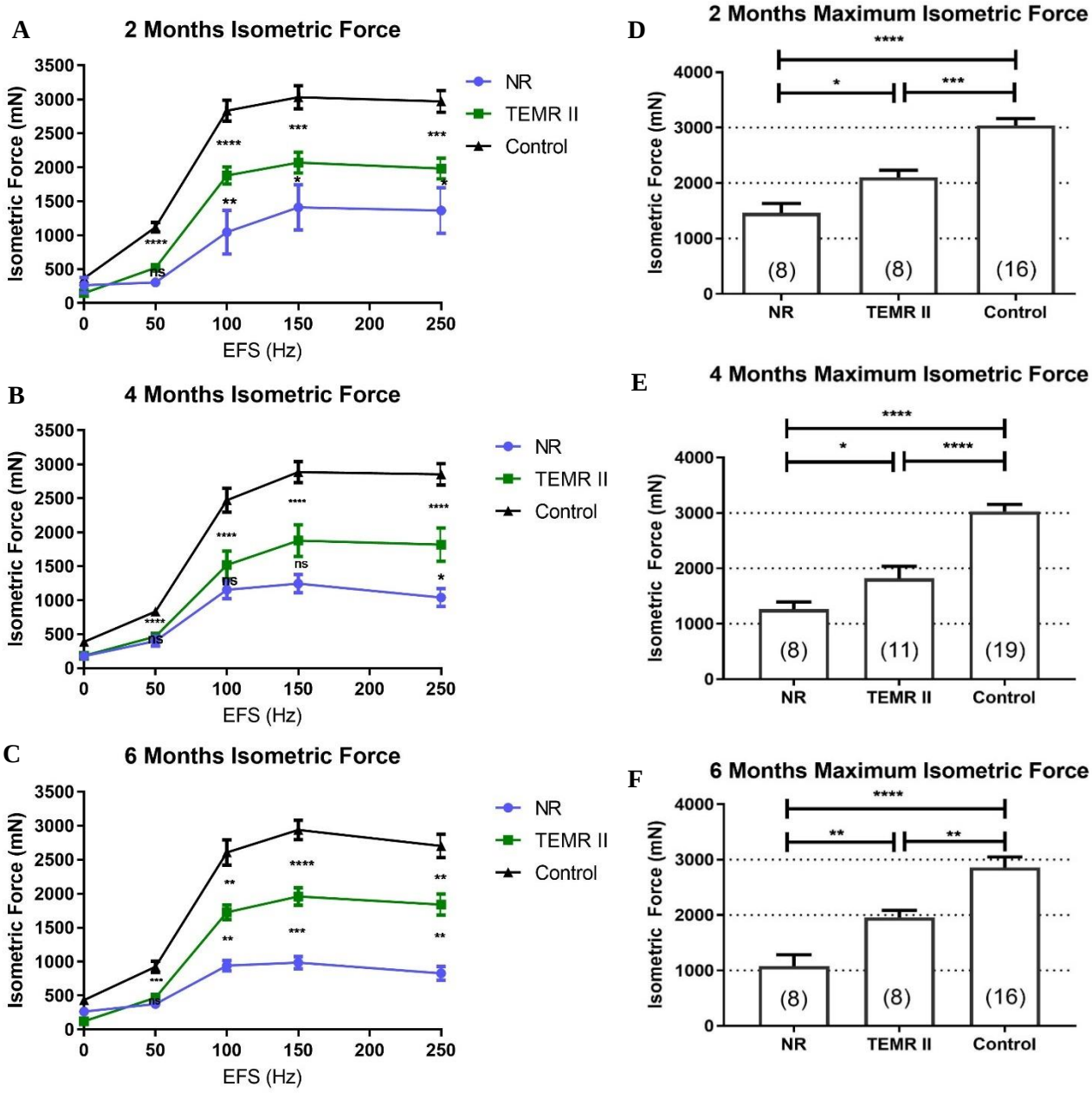

Fig 12. **Improved TEMR II isometric force production recovery is observed when compared to no repair (NR) VML injuries at 2, 4, and 6-month time points.** Measurements were taken at 50, 100, 150, and 250 Hz and represented in milli-Newtons (mN). Uninjured, injured but nonrepaired (NR), or TEMR II-repaired LD muscles were tested using direct stimulation at 35°C in an organ bath (See Methods). Isometric force as a function of stimulation frequency (A-C) was assessed for all experimental conditions at 2 months (A), 4 months (B), or 6 months (C) post injury. In A-C data, significance is shown as TEMR II against Control, and NR against TEMR II. Force-frequency curves were fit with a Hill equation. Peak isometric force production (D-F) was calculated for all experimental groups at 2 months (D), 4 months (E), and 6 months (F) time points. Values are expressed as means ± standard error (SEM). Significance is marked by * ($p<0.05$), ** ($p<0.01$), *** ($p<0.001$), and **** ($p<0.0001$). Non-significant difference is denoted by ns. Values for Isometric Force measurements are listed in Table 2.

150, and 250 Hz (Table 3). Second, peak isometric force production was calculated for all experimental groups. We plotted the average isometric force production as a function of stimulation frequency for each group (Fig. 12, A-C) and saw that in all groups, control muscles performed significantly better than the NR groups. It is also interesting to note that the TEMR II appears to create an immediate and statistically significant increase in force at the 2 month time point. At 4 and 6 months, the TEMR-treated muscles do not appear to improve, but the NR decays. It seems that might be the reason for the statistical differences at latter time points.

As hypothesized, TEMR II treated muscles out-performed NR muscles at all time points for max isometric force readings. However, I observed non-significant differences between TEMR II and NR at 4 months for 50, 100, and 150Hz which was unusual compared to any other timepoint. I have several unexplored theories for this anomaly. First, 4 additional animals were tested in the 4-month TEMR II group. This was due to an oversight in managing explant timelines. The 4 additional animals were meant to be explanted at the 2-month timepoint, but the error was not caught until the animals were 2 weeks beyond the 2 month mark. I did not want to skew the 2 month data by allowing some of the muscles to heal longer than the rest of the group, so I extended explant time to 4 months. Only 3 data points were included because one of the animals died during the explant process.

3.3.4 TEMR II versus the original TEMR

The aim of this study was to discern whether TEMR II constructs would yield significant long-term functional improvements to VML injuries in large, immune competent rat VML injury model. However, it is important to consider whether there is any merit in pursuing the additional work involved in generating TEMR II constructs when we already have demonstrated regenerative success with the original TEMR technology[5,76,93].

To this end, we compared the maximum isometric force production of the original TEMR technology to TEMR II. The maximum isometric force output of the TEMR II treated muscles didn't seem to line up to what we expected in these studies. In fact, TEMR II maximum isometric output just barely surpassed No Repair injuries created in the original TEMR study. Upon closer inspection, however, we saw something significant: the fold increase of force production, calculated as the ratio of the respective TEMR max functional isometric force production divided by the NR maximum force production, was comparable between TEMR and TEMRII studies (Fig. 13). While we cannot make direct comparisons between the two, it is an interesting observation in the right context. It appears that the VML injuries created in the TEMR II studies were more severe than those created in the original TEMR study, which may account for the decreased maximum isometric force output for the TEMR II at the same time point. This could be attributed do different size and location of the VML injury on the LD, as these factors have been shown to alter the VML response[94]. These data would seem to suggest that the TEMR II possesses comparable regenerative capacity compared to the original TEMR construct, despite initial observations of the data.

3.4 Histology

3.4.1 Muscle preparation following DMT testing

Muscles from all experimental groups were photographed (Fig. 14) and then fixed in 4% paraformaldehyde overnight at 4C after being pinned to silicone blocks. Fixed muscles were then cut horizontally across the center of the VML injury and embedded in paraffin wax (Fig. 15 A-D). Tissue sections were taken within the plane of the LD muscle and imaged as shown (Fig. 15 E). Hematoxylin and eosin stains were conducted by standard techniques to determine the basic morphology of cells in and around the implant and to observe any inflammatory response and muscle regeneration. Implants retrieved from four animals in each treatment group were studied.

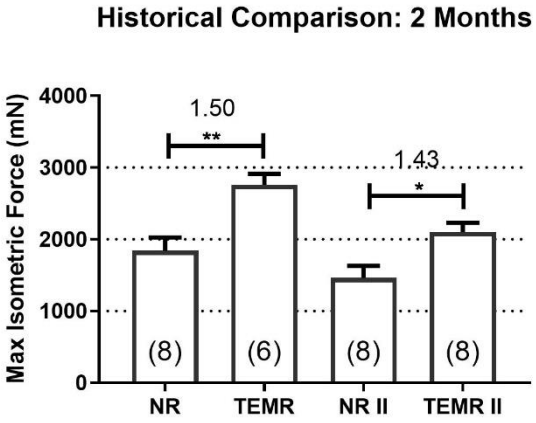

Fig 13. **TEMR II shows improved fold recovery after 6 months when compared to original TEMR technology.** Shows fold improvement of different TEMR technologies versus no repair (NR) VML injuries across studies, where after 2 months TEMR II exhibited similar fold increase in performance when compared to TEMR studies (1.42 fold improvement in TEMR II versus 1.5 fold improvement in TEMR). Fold improvement was calculated as the ratio of TEMR max functional isometric force production divided by NR max functional isometric force production and represented in milli Newtons. Significance is marked by * ($p<0.05$), ** ($p<0.01$), *** ($p<0.001$), and **** ($p<0.0001$). Non-significant difference is denoted by ns.

Sections were removed of paraffin using standard histological procedures and microwaved in Antigen retrieval solution for 20 minutes. Immunohistochemical staining was performed by using antibody to detect CD31, Smooth Muscle Actin, ED1, or ED2. After washing in PBS, cells were incubated in 488 anti-mouse IgG and 594 anti-rabbit IgG secondary antibodies when applied overnight at 4°C. Tissue sections without primary antibody were used as negative controls. Images were captured and digitized (DM4000B Leica Upright Microscope) at varying magnifications (Fig. 15 F, G). These images were only used for qualitative analysis in this thesis.

In these images, we were looking for some kind of indication of native tissue repair or regeneration. By looking at the explanted muscles, it was evident that the VML injury we created at any time point yielded significant loss of muscle. In fact, a hole was visible, even at 6 months (Fig. 14 A, C, E). This clearly demonstrates the devastation VML injury wreaks on skeletal muscle. However, when looking at TEMR II treated muscles at the same time points, you could see a filled, "healthy-looking" muscle (Fig. 14 B, D ,F). This discovery encouraged us to dig explore the mechanisms of repair in both models a little deeper.

Following the observation that TEMR II increased isometric force production in VML injuries when compared to NR injuries, we wanted to discern whether this was related to viable muscle production or some other passive force at work. To this end, we defined an Area of Injury (AOI) in each muscle of each group. We defined the AOI visually using ImageJ. The criteria for AOI included: 1) identifying areas of obvious tissue damage by looking for particularly thin or missing tissue, 2) identifying areas of regrowth at the periphery of injury by looking for smaller muscle bundles with peripherally-located nuclei. To reduce observer bias, each histological image was submitted to 2-3 other scientists and each drew two vertical lines where they perceived the AOI to be. Images were then qualitatively observed for new muscle formation within the AOI (Fig. 15 F-G).

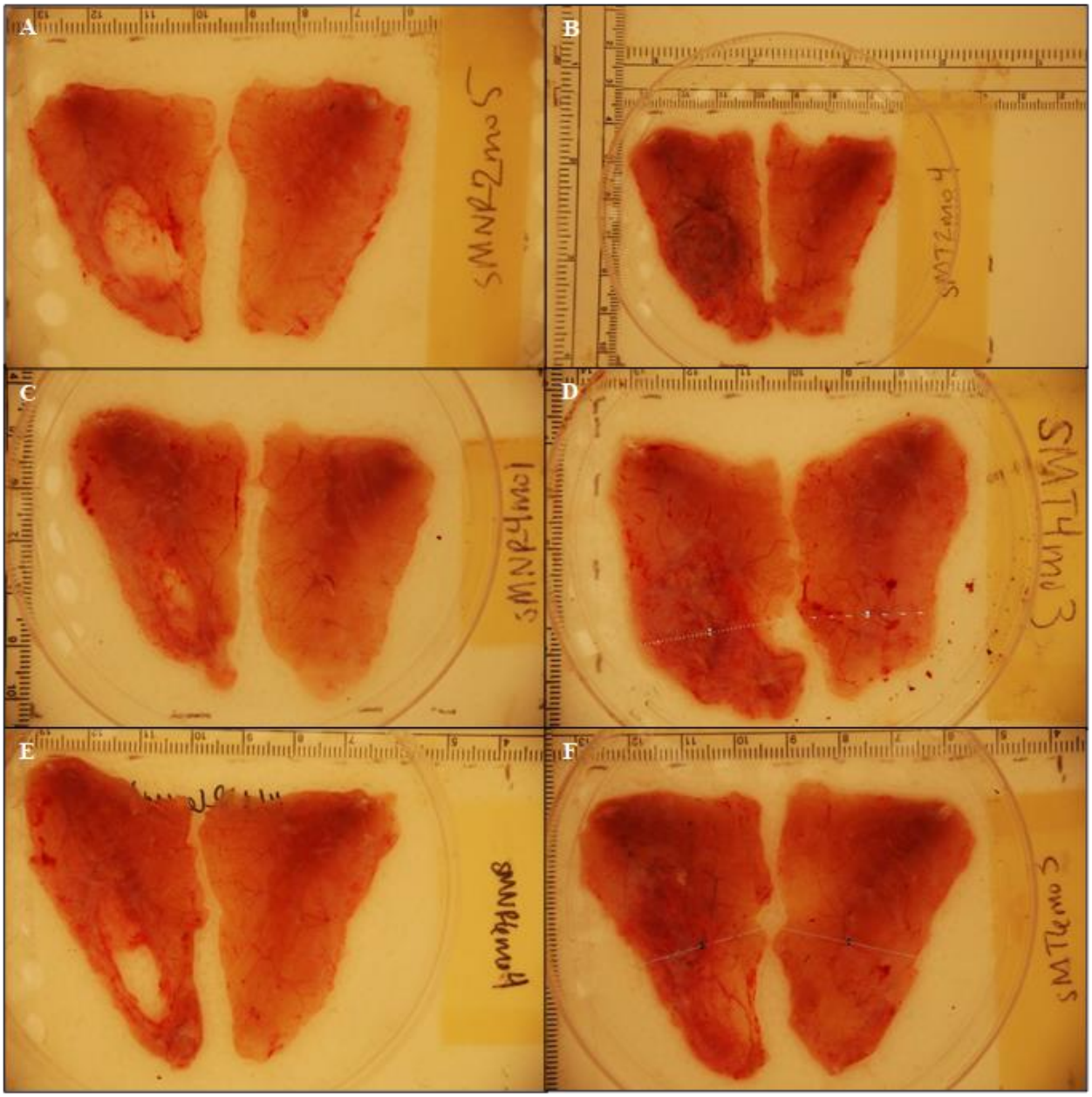

Fig 14. **Qualitative morphological improvement of TEMR II technology over NR injury.** No repair (A, C, E) and TEMR II (B, D, F) immediately post DMT organ bath testing. At 2 months (A, B), 4 months (C, D), and 6 months (E, F) there are still gaping holes in NR injuries while the TEMR II muscles appear to have vascularized, continuous muscles.

TEMR II treated muscles consistently presented with more regenerated fibers and larger over-all cross-sectional areas. One unique qualitative observation was that TEMR II treated muscles tended to lose less mass over all (Fig. 15 F, G) than NR treated muscles, which appeared to "shrivel". Although not definitive, these results encourage the conclusion that functional recovery was related to active muscle recruitment of viable muscle fibers that were regenerated, rather than passive force of the BAM.

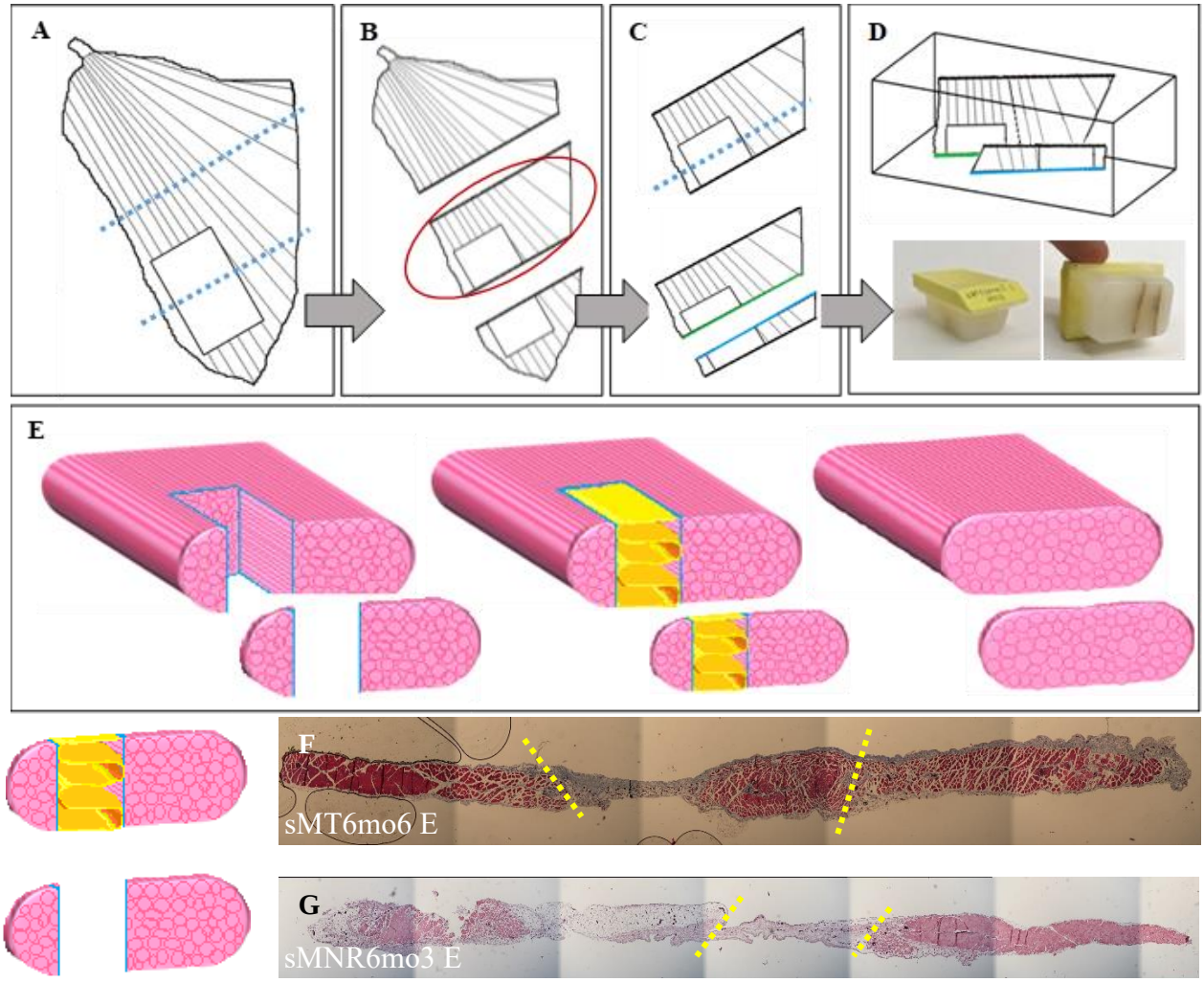

Fig 15. **Histological analysis shows markedly significant qualitative improvement of TEMR II muscles when compared to No Repair muscles.** Following 4% paraformaldehyde fixation, LD muscles were cut along the blue dotted lines shown in (A). The middle section of the muscle (B) was selected and cut again as close to the middle of the section as possible (C). The two edges of this cut were placed "down" in a paraffin embedding mold (D) so that sectioning quickly cuts into the middle of the wound area. A diagram of no repair, TEMR II, and control muscles (E, left to right) is shown to clarify what each section of the embedded muscles are expected to look like. A section of a 6-month time point TEMR II section (F) and a 6-month time point No Repair section (G) are shown. Lines demark AOI as perceived by 2-3 non-biased observers. The TEMR II muscle retains much of its shape and length when compared to the No Repair muscle.

4. Chapter 4 – Future Directions and Thoughts

Looking back, I can see many ways to make this study more robust and bulletproof. Many of these ideas may be outside of the scope of a master's student, but it is still important to consider improvements and to learn from the failures of this study.

One particular area I thought lacked the clarity and focus was in defining the success of the TEMR II technology as a successful treatment in recruiting the native tissue to regenerate. While we demonstrated that TEMR II certainly improves the functional and cosmetic outcomes of VML injuries when compared to doing nothing at all, we did little to verify that the functional recovery was due to contractile skeletal muscle. As described in the introduction, the physiology and excitation-contraction activation process of skeletal muscle are complex in their scope. A more robust experiment for successful muscle regeneration should certainly consider the following rubric:

- Identifying troponin C is present within the 'regenerated' tissue to confirm that fibers are capable of producing contractile forces.

- Confirming the presence of active neurons in the regeneration area, as neuro-muscular bundles are critical for functional success in muscle.

- Exploring the extent of angiogenesis into the regenerated area, as viable tissue is limited to the availability of oxygen and nutrients that blood vessels supply. Outside of extending the scope of this project there are many things that, if presented with the time and money, I would have liked to re-do. I think one of the most obvious criticisms that can be made of this study is the lack of direct comparison between TEMR and TEMR II. All of the TEMR data included in this study came from previous experiments. It was difficult to identify exactly what had been done in these original TEMR studies, and making direct comparisons between TEMR and TEMR II was tenuous and difficult to conceptualize. Our decision to exclude TEMR studies was grounded in the naiveté that following a protocol previously outlined by my laboratory forerunners would yield identical the injuries, thus it would not be necessary to repeat the same experiment twice. As you can see, however, there are slight variations between studies even when following painstakingly created protocols designed to mitigate variation.

Furthermore, I believe this experiment could benefit from including female rats in the VML model. This is actually something we initially attempted. Interestingly, the female TEMR II rats invariably performed worse than their male counterpoints at all time points in the study. We frequently observed that the female TEMR II injuries performed worse than female NR injuries. We hypothesized that this may have to do with the proximity of female-specific vasculature and mammary glands to our chosen VML model area. Thus, cutting out skeletal muscle in our chosen area in female rats may have created a more severe injury when compared to males, making the comparison invalid. This is a hypothesis we did not presently have the bandwidth to explore, and will be left for future students to investigate.

Other potential extensions of this study have actually been explored since my time at UVA. Notably, the LD TEMR model has been used to explore the role of passive force production generated by the TEMR in functional recovery. This information was also critical to developing a

predictive, in situ model that accurately predicts the needs of a VML injury and the response a TEMR II implant might have. Such insights can tune this platform to the specific requirements of diverse VML injuries in order to improve functional outcomes across multiple injury types.

On a final note, 3D bioprinting has rapidly expanded in scope and resolution in the last two years. Of note to this present thesis, 3D bioprinting has vast potential to improve the scalability and efficiency of the TEMR II re-seeding process, significantly reducing time and production cost. This automated process could propel the TEMR II platform (and additional skeletal muscle tissue engineering applications) to more robust and interesting heights.

4.1 Conclusions

The overriding hypothesis of this study was that TEMR IIs, made possible by specialized bioreactor preconditioning, would yield significant long-term functional improvements to VML injuries in large, immune competent muscle models. To this end, VML injuries, with or without the implanted TEMR II technology, were examined in an established murine model for their ability to enable restoration of function and native tissue morphology. We were able to demonstrate that TEMR II does, in fact, significantly improve the functional recovery of VML injuries both in the short term (2 months) and long-term (6 months) post injury. Furthermore, we had success in designing a bioreactor that made TEMR II technology possible by minimally disturbing cell layers during the re-seeding process. These successes encourage future study of this technology as a plausible solution to VML in humans.

Acknowledgements

I would like to thank my advisor, George Christ. Without him, none of this would have been possible. Furthermore, I owe a great debt of gratitude to my committee Shayn Peirce-Cottler and Don Griffin for their never-ceasing patience, flexibly, and guidance. Juliana Passipieri was integral to this work. Her guidance and friendship taught me how to "science," and ultimately, this thesis would not be half of what it is without her editorial feedback. I would also like to thank my mother for countless hours of free childcare, her emotional support, and for pushing me to complete this body of work even when I wanted to give up. And finally, all my love and gratitude to my Spawn; thank you for never, ever letting me sleep and giving me a reason to stay up late to work on this.

References

(1) Regenerative medicine - Latest research and news | Nature https://www.nature.com/subjects/regenerative-medicine (accessed May 27, 2019).

(2) NIH Fact Sheets - Regenerative Medicine https://report.nih.gov/nihfactsheets/viewfactsheet.aspx?csid=62 (accessed May 27, 2019).

(3) Corona, B. T.; Machingal, M. A.; Criswell, T.; Vadhavkar, M.; Dannahower, A. C.; Bergman, C.; Zhao, W.; Christ, G. J. Further Development of a Tissue Engineered Muscle Repair Construct In Vitro for Enhanced Functional Recovery Following Implantation In Vivo in a Murine Model of Volumetric Muscle Loss Injury. *Tissue Eng. Part A* **2012**, *18* (11–12), 1213–1228. https://doi.org/10.1089/ten.tea.2011.0614.

(4) Goldman, S. M.; Corona, B. T. Co-Delivery of Micronized Urinary Bladder Matrix Damps Regenerative Capacity of Minced Muscle Grafts in the Treatment of Volumetric Muscle Loss Injuries. *PloS One* **2017**, *12* (10), e0186593. https://doi.org/10.1371/journal.pone.0186593.

(5) Mintz, E. L.; Passipieri, J. A.; Lovell, D. Y.; Christ, G. J. Applications of In Vivo Functional Testing of the Rat Tibialis Anterior for Evaluating Tissue Engineered Skeletal Muscle Repair. *J. Vis. Exp. JoVE* **2016**, No. 116. https://doi.org/10.3791/54487.

(6) Passipieri, J. A.; Christ, G. J. The Potential of Combination Therapeutics for More Complete Repair of Volumetric Muscle Loss Injuries: The Role of Exogenous Growth Factors and/or Progenitor Cells in Implantable Skeletal Muscle Tissue Engineering Technologies. *Cells Tissues Organs* **2016**, *202* (3–4), 202–213. https://doi.org/10.1159/000447323.

(7) Chung, L.; Maestas, D. R.; Housseau, F.; Elisseeff, J. H. Key Players in the Immune Response to Biomaterial Scaffolds for Regenerative Medicine. *Adv. Drug Deliv. Rev.* **2017**, *114*, 184–192. https://doi.org/10.1016/j.addr.2017.07.006.

(8) Heymsfield, S.; Wang, Z.; Baumgartner, R.; Ross, R. *Human Body Composition: Advances in Models and Methods*; 1997; Vol. 17. https://doi.org/10.1146/annurev.nutr.17.1.527.

(9) Ehrhardt, J.; Morgan, J. Regenerative Capacity of Skeletal Muscle. *Curr. Opin. Neurol.* **2005**, *18* (5), 548–553. https://doi.org/10.1097/01.wco.0000177382.62156.82.

(10) Grogan, B. F.; Hsu, J. R.; Skeletal Trauma Research Consortium. Volumetric Muscle Loss. *J. Am. Acad. Orthop. Surg.* **2011**, *19 Suppl 1*, S35-37.

(11) Giannou, C.; Baldan, M.; Molde, Å. War Surgery Volume 2. International Committee of the Red Cross March 2013.

(12) Thiele, O. C.; Seeberger, R.; Engel, M.; Freier, K.; Hoffmann, J. Development of the Clinical Use of Distant Flaps for Head and Neck Reconstruction. *J. Cranio-Maxillo-fac. Surg. Off. Publ. Eur. Assoc. Cranio-Maxillo-fac. Surg.* **2014**, *42* (1), 79–83. https://doi.org/10.1016/j.jcms.2013.02.006.

(13) Pollot, B. E.; Corona, B. T. Volumetric Muscle Loss. In *Skeletal Muscle Regeneration in the Mouse: Methods and Protocols*; Kyba, M., Ed.; Methods in Molecular Biology; Springer New York: New York, NY, 2016; pp 19–31. https://doi.org/10.1007/978-1-4939-3810-0_2.

(14) Quintero, A. J.; Wright, V. J.; Fu, F. H.; Huard, J. Stem Cells for the Treatment of Skeletal Muscle Injury. *Clin. Sports Med.* **2009**, *28* (1), 1–11. https://doi.org/10.1016/j.csm.2008.08.009.

(15) Lieber, R. *Skeletal Muscle Structure, Function, and Plasticity*; 2011.

(16) MacIntosh, B. R.; Gardiner, P. F.; McComas, A. J. *Skeletal Muscle : Form and Function*, 2nd ed.; Champaign, IL : Human Kinetics, 2006.

(17) Megeney, L. A.; Kablar, B.; Garrett, K.; Anderson, J. E.; Rudnicki, M. A. MyoD Is Required for Myogenic Stem Cell Function in Adult Skeletal Muscle. *Genes Dev.* **1996**, *10* (10), 1173–1183. https://doi.org/10.1101/gad.10.10.1173.

(18) Gulati, A. K.; Reddi, A. H.; Zalewski, A. A. Changes in the Basement Membrane Zone Components during Skeletal Muscle Fiber Degeneration and Regeneration. *J. Cell Biol.* **1983**, *97* (4), 957–962.

(19) Turner, N. J.; Badylak, S. F. Regeneration of Skeletal Muscle. *Cell Tissue Res.* **2012**, *347* (3), 759–774. https://doi.org/10.1007/s00441-011-1185-7.
(20) Aurora, A.; Roe, J. L.; Corona, B. T.; Walters, T. J. An Acellular Biologic Scaffold Does Not Regenerate Appreciable de Novo Muscle Tissue in Rat Models of Volumetric Muscle Loss Injury. *Biomaterials* **2015**, *67*, 393–407. https://doi.org/10.1016/j.biomaterials.2015.07.040.
(21) Corona, B. T.; Wu, X.; Ward, C. L.; McDaniel, J. S.; Rathbone, C. R.; Walters, T. J. The Promotion of a Functional Fibrosis in Skeletal Muscle with Volumetric Muscle Loss Injury Following the Transplantation of Muscle-ECM. *Biomaterials* **2013**, *34* (13), 3324–3335. https://doi.org/10.1016/j.biomaterials.2013.01.061.
(22) Merritt, E. K.; Hammers, D. W.; Tierney, M.; Suggs, L. J.; Walters, T. J.; Farrar, R. P. Functional Assessment of Skeletal Muscle Regeneration Utilizing Homologous Extracellular Matrix as Scaffolding. *Tissue Eng. Part A* **2010**, *16* (4), 1395–1405. https://doi.org/10.1089/ten.TEA.2009.0226.
(23) Valentin, J. E.; Turner, N. J.; Gilbert, T. W.; Badylak, S. F. Functional Skeletal Muscle Formation with a Biologic Scaffold. *Biomaterials* **2010**, *31* (29), 7475–7484. https://doi.org/10.1016/j.biomaterials.2010.06.039.
(24) Ma, J.; Sahoo, S.; Baker, A. R.; Derwin, K. A. Investigating Muscle Regeneration with a Dermis/Small Intestinal Submucosa Scaffold in a Rat Full-Thickness Abdominal Wall Defect Model. *J. Biomed. Mater. Res. B Appl. Biomater.* **2015**, *103* (2), 355–364. https://doi.org/10.1002/jbm.b.33166.
(25) Sadtler, K.; Estrellas, K.; Allen, B. W.; Wolf, M. T.; Fan, H.; Tam, A. J.; Patel, C. H.; Luber, B. S.; Wang, H.; Wagner, K. R.; et al. Developing a Pro-Regenerative Biomaterial Scaffold Microenvironment Requires T Helper 2 Cells. *Science* **2016**, *352* (6283), 366–370. https://doi.org/10.1126/science.aad9272.
(26) Dziki, J. L.; Sicari, B. M.; Wolf, M. T.; Cramer, M. C.; Badylak, S. F. Immunomodulation and Mobilization of Progenitor Cells by Extracellular Matrix Bioscaffolds for Volumetric Muscle Loss Treatment. *Tissue Eng. Part A* **2016**, *22* (19–20), 1129–1139. https://doi.org/10.1089/ten.TEA.2016.0340.
(27) Madden, L.; Juhas, M.; Kraus, W. E.; Truskey, G. A.; Bursac, N. Bioengineered Human Myobundles Mimic Clinical Responses of Skeletal Muscle to Drugs. *eLife* **2015**, *4*, e04885. https://doi.org/10.7554/eLife.04885.
(28) Duffy, R. M.; Feinberg, A. W. Engineered Skeletal Muscle Tissue for Soft Robotics: Fabrication Strategies, Current Applications, and Future Challenges. *Wiley Interdiscip. Rev. Nanomed. Nanobiotechnol.* **2014**, *6* (2), 178–195. https://doi.org/10.1002/wnan.1254.
(29) Bian, W.; Bursac, N. Engineered Skeletal Muscle Tissue Networks with Controllable Architecture. *Biomaterials* **2009**, *30* (7), 1401–1412. https://doi.org/10.1016/j.biomaterials.2008.11.015.
(30) Nakayama, K. H.; Quarta, M.; Paine, P.; Alcazar, C.; Karakikes, I.; Garcia, V.; Abilez, O. J.; Calvo, N. S.; Simmons, C. S.; Rando, T. A.; et al. Treatment of Volumetric Muscle Loss in Mice Using Nanofibrillar Scaffolds Enhances Vascular Organization and Integration. *Commun. Biol.* **2019**, *2* (1), 1–16. https://doi.org/10.1038/s42003-019-0416-4.
(31) Passipieri, J. A.; Hu, X.; Mintz, E.; Dienes, J.; Baker, H. B.; Wallace, C. H.; Blemker, S. S.; Christ, G. J. In Silico and In Vivo Studies Detect Functional Repair Mechanisms in a Volumetric Muscle Loss Injury. *Tissue Eng. Part A* **2019**, *25* (17–18), 1272–1288. https://doi.org/10.1089/ten.tea.2018.0280.
(32) Juhas, M.; Engelmayr, G. C.; Fontanella, A. N.; Palmer, G. M.; Bursac, N. Biomimetic Engineered Muscle with Capacity for Vascular Integration and Functional Maturation in Vivo. *Proc. Natl. Acad. Sci.* **2014**, *111* (15), 5508–5513. https://doi.org/10.1073/pnas.1402723111.

(33) Serrano, A. L.; Muñoz-Cánoves, P. Regulation and Dysregulation of Fibrosis in Skeletal Muscle. *Exp. Cell Res.* **2010**, *316* (18), 3050–3058. https://doi.org/10.1016/j.yexcr.2010.05.035.
(34) Kwon, S. G.; Kwon, Y. W.; Lee, T. W.; Park, G. T.; Kim, J. H. Recent Advances in Stem Cell Therapeutics and Tissue Engineering Strategies. *Biomater. Res.* **2018**, *22*. https://doi.org/10.1186/s40824-018-0148-4.
(35) Labusca, L.; Herea, D. D.; Mashayekhi, K. Stem Cells as Delivery Vehicles for Regenerative Medicine-Challenges and Perspectives. *World J. Stem Cells* **2018**, *10* (5), 43–56. https://doi.org/10.4252/wjsc.v10.i5.43.
(36) Zhang, Z.; Gupte, M. J.; Ma, P. X. Biomaterials and Stem Cells for Tissue Engineering. *Expert Opin. Biol. Ther.* **2013**, *13* (4), 527–540. https://doi.org/10.1517/14712598.2013.756468.
(37) Scaffolds for tissue fabrication - ScienceDirect https://www.sciencedirect.com/science/article/pii/S1369702104002330 (accessed May 27, 2019).
(38) Yu, Y.; Alkhawaji, A.; Ding, Y.; Mei, J. Decellularized Scaffolds in Regenerative Medicine. *Oncotarget* **2016**, *7* (36). https://doi.org/10.18632/oncotarget.10945.
(39) Chen, T.-H. Tissue Regeneration: From Synthetic Scaffolds to Self-Organizing Morphogenesis http://www.eurekaselect.com/122019/article (accessed May 27, 2019).
(40) Pashos, N. C.; Scarritt, M. E.; Eagle, Z. R.; Gimble, J. M.; Chaffin, A.; Bunnell, B. A. Characterization of an Acellular Scaffold for a Tissue Engineering Approach to Nipple—Areolar Complex Reconstruction. *Cells Tissues Organs* **2017**, *203* (3), 183–193. https://doi.org/10.1159/000455070.
(41) Starnecker, F.; König, F.; Hagl, C.; Thierfelder, N. Tissue-Engineering Acellular Scaffolds-The Significant Influence of Physical and Procedural Decellularization Factors. *J. Biomed. Mater. Res. B Appl. Biomater.* **2018**, *106* (1), 153–162. https://doi.org/10.1002/jbm.b.33816.
(42) Ramakrishna, S.; Mayer, J.; Wintermantel, E.; Leong, K. W. Biomedical Applications of Polymer-Composite Materials: A Review. *Compos. Sci. Technol.* **2001**, *61* (9), 1189–1224. https://doi.org/10.1016/S0266-3538(00)00241-4.
(43) Nair, L. S.; Laurencin, C. T. Biodegradable Polymers as Biomaterials. *Prog. Polym. Sci.* **2007**, *32* (8), 762–798. https://doi.org/10.1016/j.progpolymsci.2007.05.017.
(44) Passive Tension - an overview | ScienceDirect Topics https://www.sciencedirect.com/topics/engineering/passive-tension (accessed May 27, 2019).
(45) Contractile Force - an overview | ScienceDirect Topics https://www.sciencedirect.com/topics/engineering/contractile-force (accessed May 27, 2019).
(46) Oragui, E.; Nannaparaju, M.; Khan, W. S. The Role of Bioreactors in Tissue Engineering for Musculoskeletal Applications. *Open Orthop. J.* **2011**, *5*, 267–270. https://doi.org/10.2174/1874325001105010267.
(47) Vunjak-Novakovic, G.; Martin, I.; Obradovic, B.; Treppo, S.; Grodzinsky, A. J.; Langer, R.; Freed, L. E. Bioreactor Cultivation Conditions Modulate the Composition and Mechanical Properties of Tissue-Engineered Cartilage. *J. Orthop. Res.* **1999**, *17* (1), 130–138. https://doi.org/10.1002/jor.1100170119.
(48) Schröder, C.; Hölzer, A.; Zhu, G.; Woiczinski, M.; Betz, O. B.; Graf, H.; Mayer-Wagner, S.; Müller, P. E. A Closed Loop Perfusion Bioreactor for Dynamic Hydrostatic Pressure Loading and Cartilage Tissue Engineering. *J. Mech. Med. Biol.* **2015**, *16* (03), 1650025. https://doi.org/10.1142/S0219519416500251.
(49) Klapper, J. A.; Thomasian, A. A.; Smith, D. M.; Gorgas, G. C.; Wunderlich, J. R.; Smith, F. O.; Hampson, B. S.; Rosenberg, S. A.; Dudley, M. E. Single-Pass, Closed-System Rapid Expansion of Lymphocyte Cultures for Adoptive Cell Therapy. *J. Immunol. Methods* **2009**, *345* (1–2), 90–99. https://doi.org/10.1016/j.jim.2009.04.009.

(50) Bancroft, G. N.; Sikavitsas, V. I.; Mikos, A. G. Technical Note: Design of a Flow Perfusion Bioreactor System for Bone Tissue-Engineering Applications. *Tissue Eng.* **2003**, *9* (3), 549–554. https://doi.org/10.1089/107632703322066723.

(51) Sikavitsas, V. I.; Bancroft, G. N.; Holtorf, H. L.; Jansen, J. A.; Mikos, A. G. Mineralized Matrix Deposition by Marrow Stromal Osteoblasts in 3D Perfusion Culture Increases with Increasing Fluid Shear Forces. *Proc. Natl. Acad. Sci. U. S. A.* **2003**, *100* (25), 14683–14688. https://doi.org/10.1073/pnas.2434367100.

(52) Cerino, G.; Gaudiello, E.; Grussenmeyer, T.; Melly, L.; Massai, D.; Banfi, A.; Martin, I.; Eckstein, F.; Grapow, M.; Marsano, A. Three Dimensional Multi-Cellular Muscle-like Tissue Engineering in Perfusion-Based Bioreactors. *Biotechnol. Bioeng.* **2016**, *113* (1), 226–236. https://doi.org/10.1002/bit.25688.

(53) Cimetta, E.; Flaibani, M.; Mella, M.; Serena, E.; Boldrin, L.; De Coppi, P.; Elvassore, N. Enhancement of Viability of Muscle Precursor Cells on 3D Scaffold in a Perfusion Bioreactor. *Int. J. Artif. Organs* **2007**, *30* (5), 415–428. https://doi.org/10.1177/039139880703000509.

(54) Vunjak-Novakovic, G.; Searby, N.; Luis, J. D.; Freed, L. E. Microgravity Studies of Cells and Tissues. *Ann. N. Y. Acad. Sci.* **2002**, *974* (1), 504–517. https://doi.org/10.1111/j.1749-6632.2002.tb05927.x.

(55) Slentz, D. H.; Truskey, G. A.; Kraus, W. E. Effects of Chronic Exposure to Simulated Microgravity on Skeletal Muscle Cell Proliferation and Differentiation. *In Vitro Cell. Dev. Biol. Anim.* **2001**, *37* (3), 148–156. https://doi.org/10.1290/1071-2690(2001)037<0148:EOCETS>2.0.CO;2.

(56) Molnar, G.; Schroedl, N. A.; Gonda, S. R.; Hartzell, C. R. Skeletal Muscle Satellite Cells Cultured in Simulated Microgravity. *Vitro Cell. Dev. Biol. - Anim.* **1997**, *33* (5), 386–391. https://doi.org/10.1007/s11626-997-0010-9.

(57) Gooch, K.; Kwon, J.; Blunk, T.; Langer, R.; Freed, L.; Vunjak-Novakovic, G. Effects of Mixing Intensity on Tissue-Engineered Cartilage. *Biotechnol. Bioeng.* **2001**, *72*, 402–407. https://doi.org/10.1002/1097-0290(20000220)72:43.0.CO;2-Q.

(58) Vunjak-Novakovic, G.; Freed, L. E.; Biron, R. J.; Langer, R. Effects of Mixing on the Composition and Morphology of Tissue-Engineered Cartilage; 1996. https://doi.org/10.1002/aic.690420323.

(59) Bardouille, C.; Lehmann, J.; Heimann, P.; Jockusch, H. Growth and Differentiation of Permanent and Secondary Mouse Myogenic Cell Lines on Microcarriers. *Appl. Microbiol. Biotechnol.* **2001**, *55* (5), 556–562. https://doi.org/10.1007/s002530100595.

(60) Weidenhamer, N. K.; Tranquillo, R. T. Influence of Cyclic Mechanical Stretch and Tissue Constraints on Cellular and Collagen Alignment in Fibroblast-Derived Cell Sheets. *Tissue Eng. Part C Methods* **2013**, *19* (5), 386–395. https://doi.org/10.1089/ten.tec.2012.0423.

(61) Riehl, B. D.; Park, J.-H.; Kwon, I. K.; Lim, J. Y. Mechanical Stretching for Tissue Engineering: Two-Dimensional and Three-Dimensional Constructs. *Tissue Eng. Part B Rev.* **2012**, *18* (4), 288–300. https://doi.org/10.1089/ten.teb.2011.0465.

(62) Cezar, C. A.; Mooney, D. J. Biomaterial-Based Delivery for Skeletal Muscle Repair. *Adv. Drug Deliv. Rev.* **2015**, *84*, 188–197. https://doi.org/10.1016/j.addr.2014.09.008.

(63) Hornberger, T. A.; Armstrong, D. D.; Koh, T. J.; Burkholder, T. J.; Esser, K. A. Intracellular Signaling Specificity in Response to Uniaxial vs. Multiaxial Stretch: Implications for Mechanotransduction. *Am. J. Physiol. Cell Physiol.* **2005**, *288* (1), C185-194. https://doi.org/10.1152/ajpcell.00207.2004.

(64) Kumar, A.; Chaudhry, I.; Reid, M. B.; Boriek, A. M. Distinct Signaling Pathways Are Activated in Response to Mechanical Stress Applied Axially and Transversely to Skeletal Muscle Fibers. *J. Biol. Chem.* **2002**, *277* (48), 46493–46503. https://doi.org/10.1074/jbc.M203654200.

(65) Kumar, A.; Murphy, R.; Robinson, P.; Wei, L.; Boriek, A. M. Cyclic Mechanical Strain Inhibits Skeletal Myogenesis through Activation of Focal Adhesion Kinase, Rac-1 GTPase, and NF-KB Transcription Factor. *FASEB J.* **2004**, *18* (13), 1524–1535. https://doi.org/10.1096/fj.04-2414com.

(66) Vandenburgh, H.; Kaufman, S. In Vitro Model for Stretch-Induced Hypertrophy of Skeletal Muscle. *Science* **1979**, *203* (4377), 265–268. https://doi.org/10.1126/science.569901.
(67) Vandenburgh, H. H.; Karlisch, P. Longitudinal Growth of Skeletal Myotubes in Vitro in a New Horizontal Mechanical Cell Stimulator. *Vitro Cell. Dev. Biol. J. Tissue Cult. Assoc.* **1989**, *25* (7), 607–616.
(68) Moon, D. G.; Christ, G.; Stitzel, J. D.; Atala, A.; Yoo, J. J. Cyclic Mechanical Preconditioning Improves Engineered Muscle Contraction. *Tissue Eng. Part A* **2008**, *14* (4), 473–482. https://doi.org/10.1089/tea.2007.0104.
(69) Matsumoto, T.; Sasaki, J.-I.; Alsberg, E.; Egusa, H.; Yatani, H.; Sohmura, T. Three-Dimensional Cell and Tissue Patterning in a Strained Fibrin Gel System. *PLoS ONE* **2007**, *2* (11). https://doi.org/10.1371/journal.pone.0001211.
(70) Powell, C. A.; Smiley, B. L.; Mills, J.; Vandenburgh, H. H. Mechanical Stimulation Improves Tissue-Engineered Human Skeletal Muscle. *Am. J. Physiol.-Cell Physiol.* **2002**, *283* (5), C1557–C1565. https://doi.org/10.1152/ajpcell.00595.2001.
(71) Cezar, C. A.; Roche, E. T.; Vandenburgh, H. H.; Duda, G. N.; Walsh, C. J.; Mooney, D. J. Biologic-Free Mechanically Induced Muscle Regeneration. *Proc. Natl. Acad. Sci.* **2016**, 201517517. https://doi.org/10.1073/pnas.1517517113.
(72) Corona, B. T.; Ward, C. L.; Baker, H. B.; Walters, T. J.; Christ, G. J. Implantation of in Vitro Tissue Engineered Muscle Repair Constructs and Bladder Acellular Matrices Partially Restore in Vivo Skeletal Muscle Function in a Rat Model of Volumetric Muscle Loss Injury. *Tissue Eng. Part A* **2014**, *20* (3–4), 705–715. https://doi.org/10.1089/ten.TEA.2012.0761.
(73) Plunkett, N.; O'Brien, F. J. Bioreactors in Tissue Engineering. *Technol. Health Care* **2011**, *19* (1), 55–69. https://doi.org/10.3233/THC-2011-0605.
(74) Machingal, M. A.; Corona, B. T.; Walters, T. J.; Kesireddy, V.; Koval, C. N.; Dannahower, A.; Zhao, W.; Yoo, J. J.; Christ, G. J. A Tissue-Engineered Muscle Repair Construct for Functional Restoration of an Irrecoverable Muscle Injury in a Murine Model. *Tissue Eng. Part A* **2011**, *17* (17–18), 2291–2303. https://doi.org/10.1089/ten.tea.2010.0682.
(75) Kesireddy, V. Evaluation of Adipose-Derived Stem Cells for Tissue-Engineered Muscle Repair Construct-Mediated Repair of a Murine Model of Volumetric Muscle Loss Injury. *Int. J. Nanomedicine* **2016**, *11*, 1461–1473. https://doi.org/10.2147/IJN.S101955.
(76) Mintz, E. L.; Passipieri, J. A.; Franklin, I. R.; Toscano, V. M.; Afferton, E. C.; Sharma, P. R.; Christ, G. J. Long-Term Evaluation of Functional Outcomes Following Rat Volumetric Muscle Loss Injury and Repair. *Tissue Eng. Part A* **2019**. https://doi.org/10.1089/ten.TEA.2019.0126.
(77) Adductor Pollicis Muscle. *Wikipedia*; 2018.
(78) Latissimus Dorsi Muscle. *Wikipedia*; 2019.
(79) Miar, S.; Shafiee, A.; Guda, T.; Narayan, R. Additive Manufacturing for Tissue Engineering. In *3D Printing and Biofabrication*; Ovsianikov, A., Yoo, J., Mironov, V., Eds.; Reference Series in Biomedical Engineering; Springer International Publishing: Cham, 2018; pp 1–52. https://doi.org/10.1007/978-3-319-40498-1_2-1.
(80) Doyle, K. Bioprinting: From Patches to Parts. *Genet. Eng. Biotechnol. News* **2014**, *34* (10), 1, 34–35. https://doi.org/10.1089/gen.34.10.02.
(81) Kim, J. H.; Seol, Y.-J.; Ko, I. K.; Kang, H.-W.; Lee, Y. K.; Yoo, J. J.; Atala, A.; Lee, S. J. 3D Bioprinted Human Skeletal Muscle Constructs for Muscle Function Restoration. *Sci. Rep.* **2018**, *8* (1), 12307. https://doi.org/10.1038/s41598-018-29968-5.
(82) Mozetic, P.; Giannitelli, S. M.; Gori, M.; Trombetta, M.; Rainer, A. Engineering Muscle Cell Alignment through 3D Bioprinting. *J. Biomed. Mater. Res. A* **2017**, *105* (9), 2582–2588. https://doi.org/10.1002/jbm.a.36117.

(83) Juhas, M.; Ye, J.; Bursac, N. Design, Evaluation, and Application of Engineered Skeletal Muscle. *Methods San Diego Calif* **2016**, *99*, 81–90. https://doi.org/10.1016/j.ymeth.2015.10.002.
(84) Criswell, T. L.; Corona, B. T.; Wang, Z.; Zhou, Y.; Niu, G.; Xu, Y.; Christ, G. J.; Soker, S. The Role of Endothelial Cells in Myofiber Differentiation and the Vascularization and Innervation of Bioengineered Muscle Tissue in Vivo. *Biomaterials* **2013**, *34* (1), 140–149. https://doi.org/10.1016/j.biomaterials.2012.09.045.
(85) Levenberg, S.; Rouwkema, J.; Macdonald, M.; Garfein, E. S.; Kohane, D. S.; Darland, D. C.; Marini, R.; Blitterswijk, C. A. van; Mulligan, R. C.; D'Amore, P. A.; et al. Engineering Vascularized Skeletal Muscle Tissue. *Nat. Biotechnol.* **2005**, *23* (7), 879. https://doi.org/10.1038/nbt1109.
(86) Contrast-limited adaptive histogram equalization (CLAHE) - MATLAB adapthisteq https://www.mathworks.com/help/images/ref/adapthisteq.html#bviewhb (accessed Oct 28, 2018).
(87) Suppress light structures connected to image border - MATLAB imclearborder https://www.mathworks.com/help/images/ref/imclearborder.html (accessed Oct 28, 2018).
(88) 2-D adaptive noise-removal filtering - MATLAB wiener2 https://www.mathworks.com/help/images/ref/wiener2.html (accessed Oct 28, 2018).
(89) Convert image to binary image, based on threshold - MATLAB im2bw https://www.mathworks.com/help/images/ref/im2bw.html (accessed Oct 28, 2018).
(90) Fill image regions and holes - MATLAB imfill https://www.mathworks.com/help/images/ref/imfill.html (accessed Oct 28, 2018).
(91) Morphologically open image - MATLAB imopen https://www.mathworks.com/help/images/ref/imopen.html (accessed Oct 28, 2018).
(92) Remove small objects from binary image - MATLAB bwareaopen https://www.mathworks.com/help/images/ref/bwareaopen.html (accessed Oct 28, 2018).
(93) Juliana Passipieri; Ellen Mintz; Hannah B. Baker; Jack Dienes; Kimberly Smith; David Remer; George Christ. Tissue Engineered Muscle Repair (TEMR) for Treatment of a Critically Sized VML Injury. *Tissue Eng. Part A* **2017**, *23*.
(94) Westman, A. M.; Dyer, S. E.; Remer, J. D.; Hu, X.; Christ, G. J.; Blemker, S. S. A Coupled Framework of in Situ and in Silico Analysis Reveals the Role of Lateral Force Transmission in Force Production in Volumetric Muscle Loss Injuries. *J. Biomech.* **2019**, *85*, 118–125. https://doi.org/10.1016/j.jbiomech.2019.01.025.